Wiley
Advances in Mathematical Physics
Volume 2024, Article ID 6420467, 23 pages
https://doi.org/10.1155/2024/6420467

Research Article

Modulation Instability, Analytical, and Numerical Studies for Integrable Time Fractional Nonlinear Model through Two Explicit Methods

Md. Mamunur Roshid[1,2] **Mosfiqur Rahman**[2] **Mahtab Uddin**[3] **and Harun Or Roshid**[4]

[1]*Department of Mathematics, Hamdard University Bangladesh, Munshigonj, Bangladesh*
[2]*Department of Textile Engineering, Uttara University, Dhaka, Bangladesh*
[3]*Institute of Natural Sciences, United International University, Dhaka, Bangladesh*
[4]*Department of Mathematics, Sunamganj Science and Technology University, Sunamganj, Bangladesh*

Correspondence should be addressed to Mahtab Uddin; mahtab@ins.uiu.ac.bd

Received 15 March 2024; Revised 26 April 2024; Accepted 3 August 2024

Academic Editor: Onur Alp Ilhan

The present work deals with the investigation of the time-fractional Klein–Gordon (K-G) model, which has great importance in theoretical physics with applications in various fields, including quantum mechanics and field theory. The main motivation of this work is to analyze modulation instability and soliton solution of the time-fractional K-G model. Comparative studies are investigated by β-fraction derivative and M-fractional derivative. For this purpose, we used unified and advanced $\exp(-\phi(\xi))$-expansion approaches that are highly important tools to solve the fractional model and are used to create nonlinear wave pattern (both solitary and periodic wave) solutions for the time-fractional K-G model. For the special values of constraints, the periodic waves, lumps with cross-periodic waves, periodic rogue waves, singular soliton, bright bell shape, dark bell shape, kink and antikink shape, and periodic wave behaviors are some of the outcomes attained from the obtained analytic solutions. The acquired results will be useful in comprehending the time-fractional K-G model's dynamical framework concerning associated physical events. By giving specific values to the fractional parameters, graphs are created to compare the fractional effects for the β-fraction derivative and M-fractional derivative. Additionally, the modulation instability spectrum is expressed utilizing a linear analysis technique, and the modulation instability bands are shown to be influenced by the third-order dispersion. The findings indicate that the modulation instability disappears for negative values of the fourth order in a typical dispersion regime. Consequently, it was shown that the techniques mentioned previously could be an effective tool to generate unique, precise soliton solutions for numerous uses, which are crucial to theoretical physics. This work provided the effect of the recently updated two fraction forms, and in the future, we will integrate the space–time M-fractional form of the governing model by using the extended form of the Kudryashov method. Maple 18 is utilized as the simulation tool.

1. Introduction

Numerous theoretical and scientific fields, including plasma physics, fluid dynamics, the study of materials, biosciences, optical fiber telecommunications, the physics of solid states, and many more [1, 2, 3, 4, 5, 6], deal with nonlinear systems. In many areas of mathematical physics and engineering, exact solutions to these nonlinear systems are crucial in presenting some complex happenings. A lot of work has recently been performed to provide a paradigm for the new, exact, and explicit solutions of the NFPDEs. To obtain the approximative, exact, and explicit solutions to these nonlinear equations, numerous potent strategies have been proposed, such as the fractional residual method [7], a new multistage procedure [4], a new analytical procedure [8], EMSE method [5], Darboux–Crum transformations and Hirota's direct technique [9], modified simple equation method [6, 10], reduced differential transform method [11], ansatz function method [12], improved extended auxiliary equation method [13], discrete algebraic framework [14], IRM-CG method [15], transformed rational function method [16], the residual technique [17], a new multistage technique [18], new analytical technique [19], φ^6-expansion and MGERF procedure [20], two variable (G′/G,/G)-expansion method [21], improved Bernoulli subequation function approach [22], extended tanh-function method [23], Hirota bilinear [24], the unified auxiliary equation method [25], auxiliary equation technique [26], Hirota bilinear [27], advance exponential expansion method [28], sine-Gordon expansion method [29], extending DT iteration algorithm [30], novel analytical technique [31], novel (G'/G)-expansion method [32], modified exp-function method [33, 34], ERS-C and ERSh-Ch procedures [35], modified Kudryashov method [36], R-B sub-ODE technique [37], unified method [38], Lie symmetry analysis [39], SE and NMK technique [40], extended direct algebraic technique [41], generalized projective Riccati method [42], Sardar subequation method [43], exp $(-\Phi\ (\xi))$-expansion method [44], extended sinh-Gordon equation expansion method [45], new extended auxiliary equation method and the extended Kudryashov method [46], generalized unified method [47, 48], and so many.

In the discipline of nonlinear modeling, fractional calculus—a branch of mathematics that deals with integrals as well as derivatives of noninteger orders—has grown in significance. Its significance lies in its ability to provide a more accurate representation of complex physical phenomena that cannot be adequately described using traditional integer-order calculus. This note explores the pivotal role of fractional calculus in nonlinear modeling while emphasizing its importance and its impact on various fields. In the nonlinear differential model, the fraction calculus is most important in explaining diverse complex phenomena. Fractional differential equations (FDEs) are a natural extension of traditional differential equations. They have found applications in various fields, including mathematical physics [49, 50, 51], engineering [52], finance [53, 54], and biology [55]. FDEs enable the modeling of complex phenomena with fractional-order dynamics, allowing for more accurate predictions and insights.

In this article, we explain some dynamical nature of the M-fractional derivative Klein–Gordon (K-G) equation in the resulting form:

$$ {}_kD_{M,t}^{2\chi,\psi} L - \alpha^2 L_{xx} + \beta L - mL^2 = 0. \tag{1}$$

Here, $L = L(x, t)$ is the wave function with $L_{xx} = \frac{\partial^2 L(x,t)}{\partial x^2}$, and ${}_kD_{M,t}^{\chi,\psi}$ is M-fractional derivative operator, and α represents the characteristic momentum associated with the system. It determines the spread of the wavefunction in momentum space, reflecting the spatial extent of the particle's wave packet, and β Signifies the potential energy contribution to the dynamics of the system. It influences the behavior of the scalar field and its interaction with other fields, contributing to the overall energy balance, and m denotes the mass of the scalar particle. It governs the particle's inertia and its response to external forces, profoundly influencing its dynamics and stability. The K-G model finds applications across various fields, including quantum field theory, solid-state physics, and cosmology. In quantum field theory, it describes scalar particles like mesons, elucidating their behavior in particle interactions. In solid-state physics, it is utilized to analyze lattice vibrations (phonons) and defects in crystals.

In the last centuries, various influential and dominant strategies have been proposed to implement the K-G equation solutions, such as the Adomian decomposition procedure [56], the auxiliary equation scheme [57], the method of normal forms of Shatah [58], and Exp-function scheme [59]. The main motivation of this manuscript is to analyze the modulation instability and integrate some soliton solution of the time-fractional K-G model. Modulation instability provides crucial insights into the behavior of nonlinear systems. By studying how small perturbations can grow and evolve into complex patterns, researchers gain a deeper understanding of the underlying dynamics governing the system. To execute the soliton solutions, we apply two dynamical methods, namely, the unified method and advanced $\exp(-\phi(\xi))$-expansion method to find the soliton wave pattern of the time-fractional K-G model. For analyzing the effect of fractional parameters, we use two novel fractional derivative forms, namely, time M-fractional and β time-fractional derivatives, and also compared between these fractions.

We split this article into seven sections. The introduction section is our Section 1. In Section 2, the working procedure of unified and advanced $\exp(-\phi(\xi))$-expansion approaches is enlightened, whereas we implemented the unified and advanced $\exp(-\phi(\xi))$-expansion approaches into the nonlinear quadratic model stated in Section 3. In Section 4, graphical representation and discussions are conveyed, whereas comparative analysis and novelty of this work are discussed in Section 5. In Section 6, the modulation instability is done, and in Section 7, the overview of this work is provided.

2. Method and Material

Fractional derivatives find extensive applications across diverse scientific and engineering domains due to their ability to capture nonlocal and memory-dependent effects, offering a more accurate description of complex phenomena. In physics, fractional derivatives play a crucial role in modeling anomalous diffusion processes, such as subdiffusion and superdiffusion, observed in porous media, biological tissues, and financial markets. By incorporating fractional derivatives into diffusion equations, scientists can better understand the transport of particles in heterogeneous environments, leading to advancements in drug delivery systems, groundwater flow modeling, and pollutant dispersion analysis. Recently, many researchers developed the fractional derivative form. β- and M-fractional derivative one of them and the latest version of fractional derivative.

2.1. Definition and Some Features of β-Fractional Derivative. The technical description of the β-derivative is [60, 61]

$$ {}_0^A D_t^n \{H(t)\} = \lim_{\epsilon \to 0} \frac{H\left(t + \epsilon \left(t + \frac{1}{T(n)}\right)^{1-n}\right) - H(t)}{\epsilon}. \tag{2}$$

2.1.1. Essential Features

(i) Let θ and ϑ are the real numbers, $n \neq 0$ and H are two β-differentiable functions, and $\beta \in (0,1]$, and then ${}_0^A D_t^n \{\theta R(t) + \vartheta S(t)\} = \theta {}_0^A D_t^n R(t) + \vartheta {}_0^A D_t^n S(t)$.

(ii) ${}_0^A D_t^n \{C\} = 0$, where C is constant.

(iii) ${}_0^A D_t^n \{R(t) \cdot S(t)\} = S(t) {}_0^A D_t^n \{R(t)\} + R(t) {}_0^A D_t^n \{S(t)\}$.

(iv) ${}_0^A D_t^n (\frac{R(t)}{S(t)}) = \frac{S(t) {}_0^A D_t^n \{R(t)\} - R(t) {}_0^A D_t^n \{S(t)\}}{S^2(t)}$, considering $\varepsilon = (t + \frac{1}{T(n)})^{n-1} h$, and $h \to 0$, when $\varepsilon \to 0$, consequently.

(v) ${}_0^A D_t^n R(t) = (t + \frac{1}{\Gamma(n)})^{1-n} \frac{dR(t)}{dt}$, with $\xi = \frac{l}{n}(t + \frac{1}{\Gamma(n)})^n$, where l is a constant.

(vi) ${}_0^A D_t^n (R(\xi)) = l \frac{dR(\xi)}{d\xi}$.

Atangana provided the evidence for the aforementioned relationships in [61].

2.2. Definition and Some Features of M-Fractional Derivative. Oliveira and Sousa introduced the M-fractional derivation [62] as a brandnew variation of the fractional derivative. The M-fractional derivative provides a more flexible alternative by getting rid of the restrictions of traditional derivatives.

Definition 1. Given a function $\varphi : [0, \infty) \to (-\infty, \infty)$ and an order, M-fractional derivative is defined as follows:

$$ {}_k D_{M,t}^{\chi,\phi} \varphi = \lim_{\epsilon \to 0} \frac{\varphi\left(t_\kappa \phi_\psi (\epsilon t^{-\chi})\right) - \varphi(t)}{\epsilon}, t > 0, \psi > 0. \quad (3)$$

Here, $\phi_\psi(x)$ is a truncated Mittag-Leffler function of one parameter, defined as [62, 63, 64], and taking values in the interval $(0, 1)$:

$$\phi_\psi(x) = \sum_{n=0}^{k} \frac{x^n}{\Gamma(\phi n + 1)}. \quad (4)$$

2.2.1. Characteristics. Suppose that $0 < \chi \leq 1$, and $l, m \to \Re$. Let u, v be functions that are $\chi-$ differentiable at a point $t > 0$. Then

(1) ${}_k D_{M,t}^{\chi,\psi} (lF + mG) = l\, {}_k D_{M,t}^{\chi,\psi} (F) + m\, {}_k D_{M,t}^{\chi,\psi} (G)$.

(2) ${}_k D_{M,t}^{\chi,\psi} (FvG) = F\, {}_k D_{M,t}^{\chi,\psi} (G) + G\, {}_k D_{M,t}^{\chi,\psi} (F)$.

(3) ${}_k D_{M,t}^{\chi,\psi} (\frac{F}{G}) = \frac{G\, {}_k D_{M,t}^{\chi,\psi} (F) - F\, {}_k D_{M,t}^{\chi,\psi} (G)}{G^2}$.

(4) ${}_k D_{M,t}^{\chi,\psi} (t^{\varpi}) = \varpi t^{\varpi - \chi}$, $\varpi \varepsilon \Re$.

(5) ${}_k D_{M,t}^{\chi,\psi} (c) = 0$, $c\, \varepsilon\, \Re$.

(6) ${}_k D_{M,t}^{\chi,\psi} (F \circ G) = F'(G)\, {}_k D_{M,t}^{\chi,\psi} G(t)$, for F is differentiable at G.

(7) ${}_k D_{M,t}^{\chi,\psi} F(t) = \frac{t^{1-\chi}}{\Gamma(\psi+1)} \frac{dF}{dt}$, for F is differentiable.

Remarks. Assuming that u is a $\chi-$ differentiable in the interval $(0, p)$, where $p > 0$, then the following holds:

$$ {}_k D_{M,t}^{\chi,\psi} F(0) = \lim_{t \to 0^+} \left({}_k D_{M,t}^{\chi,\psi} F(t) \right). \quad (5)$$

2.3. Analytical Method. This section will provide a general explanation of the unified technique [64, 65] and the advanced $\exp(-\phi(\eta))$-expansion method [66]. These methods are both newly launched. By implementing the unified method, we get more (nine solutions) exact and analytic solutions. This method provided some novel solution because the maximum method expressed the solutions of this auxiliary differential equation in terms of tanh/coth andtan/cot function, but in this method, the solutions combine of sin and cos , sinh and cosh functions, or only sin /cos and sinh/cosh. So unified method has some novel properties. Similarly, the advanced $\exp(-\phi(\eta))$-expansion method has a novel auxiliary differential equation and has some novel and linear solution to execute some novel phenomena. The main limitation of the unified and advanced $\exp(-\phi(\eta))$-expansion methods are both methods that cannot be calculated the solution directly such as the modified simple equation method [47]. They used some predefined solutions of their respective auxiliary differential equations. All equations cannot be solved by using unified and advanced $\exp(-\phi(\eta))$-expansion methods such as modified Oskolkov equation [48]. We initially presume a nonlinear model for $L = L(x, t)$, in the following form:

$$G(L_{xt}, L_t, L^2, L_{xxx} \ldots\ldots\ldots\ldots) = 0. \quad (6)$$

Inserting the variable $\eta = kx \pm \omega t; L(x, t) = U(\eta)$ into Equation (6) to get the ordinary form of Equation (6) is as follows:

$$f_1\left(-k\omega U_{\eta\eta}, -\omega U_\eta, U^2, k^2 U_{\eta\eta\eta}, \ldots\ldots\right) = 0. \quad (7)$$

2.3.1. Unified Technique. Let us attempt to determine the solutions to Equation (7) in the following manner:

$$\mathrm{U}(\eta) = \sum_{J=0}^{M} \mathrm{p}_J F(\eta)^J + \sum_{i=1}^{M} \frac{\mathrm{q}_i}{F(\eta)^i}, \quad (8)$$

where M is a free positive integer and θ_i and ϑ_i for $(0 \leq i \leq M)$ are discovered afterward.

The solution in Equation (8) satisfied the following auxiliary equation:

$$\frac{d\mathrm{F}(\eta)}{d\eta} = \lambda + F(\eta)^2. \quad (9)$$

The solutions of the auxiliary equation are as follows:

If $\lambda > 0$, then we get

$$F(\chi) = \begin{cases} \dfrac{\sqrt{(\varepsilon^2 - \kappa^2)\lambda} - \varepsilon\sqrt{\lambda}\cos\left(2\sqrt{\lambda}(\eta+h)\right)}{\varepsilon\sin\left(2\sqrt{\lambda}(\eta+h)\right)+\kappa} \\ \dfrac{-\sqrt{(\varepsilon^2 - \kappa^2)\lambda} - \varepsilon\sqrt{\lambda}\cos\left(2\sqrt{\lambda}(\eta+h)\right)}{\varepsilon\sin\left(2\sqrt{\lambda}(\eta+h)\right)+\kappa} \\ \mathrm{I}\sqrt{\lambda} - \dfrac{2I\varepsilon\sqrt{\lambda}}{\varepsilon+\cos\left(2\sqrt{\lambda}(\eta+h)\right) - \mathrm{I}\sin\left(2\sqrt{\lambda}(\eta+h)\right)} \\ \mathrm{I}\sqrt{\lambda} + \dfrac{2\varepsilon\sqrt{\lambda}}{\varepsilon+\cos\left(2\sqrt{\lambda}(\eta+h)\right) + \mathrm{I}\sin\left(2\sqrt{\lambda}(\eta+h)\right)} \end{cases}. \quad (10)$$

If $\lambda < 0$, then we get

$$F(\chi) = \begin{cases} \dfrac{\sqrt{-(\varepsilon^2 + \kappa^2)\lambda} - \varepsilon\sqrt{-\lambda}\cosh\left(2\sqrt{-\lambda}(\eta+h)\right)}{\varepsilon\sinh\left(2\sqrt{-\lambda}(\eta+h)\right)+\kappa} \\ \dfrac{-\sqrt{-(\varepsilon^2 + \kappa^2)\lambda} - \varepsilon\sqrt{-\lambda}\cosh\left(2\sqrt{-\lambda}(\eta+h)\right)}{\varepsilon\sinh\left(2\sqrt{-\lambda}(\eta+h)\right)+\kappa} \\ \sqrt{-\lambda} - \dfrac{2\varepsilon\sqrt{-\lambda}}{\varepsilon+\cosh\left(2\sqrt{-\lambda}(\eta+h)\right) - \sinh\left(2\sqrt{-\lambda}(\eta+h)\right)} \\ -\sqrt{-\lambda} + \dfrac{2\varepsilon\sqrt{-\lambda}}{\varepsilon+\cosh\left(2\sqrt{-\lambda}(\eta+h)\right) + \sinh\left(2\sqrt{-\lambda}(\eta+h)\right)} \end{cases}. \quad (11)$$

If $\lambda > 0$, then we get

$$F(\chi) = \frac{1}{\eta + h}. \quad (12)$$

The outcome of Equation (8) with the help of an auxiliary equation is inserted into the dynamic Equation (7) to have

$$P(F(\eta)) = C_0 + C_1 F(\eta)^{\pm 1} + C_2 F(\eta)^{\pm 2} + \dots + C_\tau F(\eta)^{\pm n} = 0. \quad (13)$$

The parameters $C_i (0 \le i \le n)$ in Equation (13) can be adjusted to zero to produce the following set of equations:

$$C_i = 0, i = 0, \dots, n. \quad (14)$$

To get the nontrivial solutions, we solve the obtained equation by Maple 18.

2.3.2. Advanced $\exp(-\phi(\eta))$*-Expansion Method.* The precise solution of Equation (8) is taken to be using the advanced $\exp(-\phi(\eta))$ approach:

$$U(\eta) = \sum_{J=0}^{M} \mathrm{A}_J e^{(-\phi(\eta))^J}. \quad (15)$$

The ODE in the following form is satisfied by the derivative of $\phi(\eta)$:

$$\phi'(\eta) = -\left(\theta_1 e^{(-\phi(\eta))} + \theta_2 e^{(\phi(\eta))}\right), \quad (16)$$

where θ_i are arbitrary constants. If we insert Equation (13) with Equation (15) into Equation (6), then we get $P(e^{(\phi(\eta))}) = p_0(e^{(\phi(\eta))})^0 + p_1 e^{(\phi(\eta))} + p_2(e^{(\phi(\eta))})^2 + \dots + p_n(e^{(\phi(\eta))})^n$. We set $p_0 = 0, p_1 = 0, p_2 = 0, \dots, p_n = 0$ and solve them to get the value of a_i $(i = 0, 1, 2, \dots, N)k, \omega$. The required solutions of Equation (6) can be obtained by substituting a_i, k, and ω into Equation (8).

The solution of the considering differential equation is given below:

Case 01: When $\theta_1\theta_2 > 0$

$$\begin{aligned} \phi(\eta) &= \ln\left(\sqrt{\frac{\theta_1}{\theta_2}}\tan\left(\sqrt{\theta_1\theta_2}(\eta+h)\right)\right), \text{and} \\ \phi(\eta) &= \ln\left(-\sqrt{\frac{\theta_1}{\theta_2}}\cot\left(\sqrt{\theta_1\theta_2}(\eta+h)\right)\right). \end{aligned} \quad (17)$$

Case 02: When $\theta_1\theta_2 < 0$

$$\begin{aligned} \phi(\eta) &= \ln\left(\sqrt{\frac{\theta_1}{-\theta_2}}\tanh\left(\sqrt{-\theta_1\theta_2}(\eta+h)\right)\right), \text{and} \\ \phi(\eta) &= \ln\left(\sqrt{\frac{\theta_1}{-\theta_2}}\coth\left(\sqrt{-\theta_1\theta_2}(\eta+h)\right)\right). \end{aligned} \quad (18)$$

Case 03: When $\theta_2 > 0$ and $\theta_1 = 0$

$$\phi(\xi) = \ln\left(\frac{1}{-\theta_2(\eta+h)}\right). \quad (19)$$

Case 04: When $\theta_2 = 0$ and $\theta_1 \in \mathbb{R}$

$$\phi(\xi) = \ln(\theta_1(\eta + C)). \quad (20)$$

Here, h and C are arbitrary constants.

3. Application of the Fractional Klein–Gordon Equation Model

In this section, we applied the unified technique and advanced $\exp(-\phi(\eta))$-expansion method for fractional K-G equation with nonlinear quadratic model.

3.1. Mathematical Analysis. In M-fractional form of Equation (1) is ${}_kD_{M,t}^{2p,\phi}L - \alpha^2 L_{xx} + \beta L - mL^2 = 0$.

In the β-fractional form of Equation (1), it is ${}_0^A D_t^{2p} L - \alpha^2 L_{xx} + \beta L - mL^2 = 0$.

To convert the fractional K-G equation from the partial to ordinary differential equation, we used the transformation variable $\eta = kx - \omega \frac{1}{p}(t + \frac{1}{\Gamma(n)})^p; L(x,t) = u(\eta)$ for the β-fractional form and $\eta = kx - \omega \frac{\Gamma(n+1)}{p} t^p; L(x,t) = u(\eta)$ for the M-fractional form. The ordinary form of the fractional K-G equation is

$$(-\alpha^2 k^2 + \omega^2)u'' + \beta u - mu^2 = 0. \tag{21}$$

3.2. Application of Unified Technique. According to the unified technique, the balance number M is obtained from balancing between u'' and u^2 which is $M=2$. The solution Equation (21) takes the form

$$u(\xi) = p_0 + p_1 F(\eta) + p_2 F(\eta)^2 + \frac{q_2}{F(\eta)} + \frac{q_3}{F(\eta)^2}. \tag{22}$$

According to the tanh method, inserting Equation (22) with Equation (13) into Equation (21), we get the following system of equations:

$$\begin{aligned}
&f(\eta)^4 : (-6\alpha^2 k^2 p_2 - m p_2^2 + 6w^2 p_2) = 0,\\
&f(\eta)^3 : (-2\alpha^2 k^2 p_1 - 2m p_1 p_2 + 2w^2 p_1) = 0,\\
&f(\eta)^2 : -8\alpha^2 k^2 \lambda p_2 + 8\lambda w^2 p_2 - 2m p_0 p_2 - m p_1^2 + \beta p_2 = 0,\\
&f(\eta) : (-2\alpha^2 k^2 \lambda p_1 + 2\lambda w^2 p_1 - 2m p_0 p_1 - 2m p_2 q_2 + \beta p_1 = 0,\\
&f(\eta)^0 : -2p_2 \lambda^2 \alpha^2 k^2 - 2q_3 \alpha^2 k^2 + 2p_2 \lambda^2 w^2 - m p_0^2 -\\
&2m p_1 q_2 - 2m p_2 q_3 + 2q_3 w^2 + \beta p_0 = 0,\\
&\frac{1}{f(\eta)} : -2\alpha^2 k^2 \lambda q_2 + 2\lambda w^2 q_2 - 2m p_0 q_2 - 2m p_1 q_3 + \beta q_2 = 0,\\
&\frac{1}{f(\eta)^2} : -8\alpha^2 k^2 \lambda q_3 + 8\lambda w^2 q_3 - 2m p_0 q_3 - m q_2^2 + \beta q_3 = 0,\\
&\frac{1}{f(\eta)^3} : -2\alpha^2 k^2 \lambda^2 q_2 + 2\lambda^2 w^2 q_2 - 2m q_2 q_3 = 0,\\
&\frac{1}{f(\eta)^4} : -6\alpha^2 k^2 \lambda^2 q_3 + 6\lambda^2 w^2 q_3 - m q_3^2 = 0.
\end{aligned}$$

After using Maple to solve the aforementioned system of equations, the following four sets of solutions will be obtained.

Case 01: $\omega = \sqrt{\frac{16k^2\alpha^2\lambda - \beta}{16\lambda}}, p_0 = -\frac{-\beta}{4m}, q_2 = p_1 = 0, p_2 = -\frac{6\beta}{16\lambda m}, q_3 = -\frac{6\beta\lambda}{16m}$.

For $\lambda > 0$, the trigonometric solutions are

$$u(\eta) = \frac{\beta}{4m} + \frac{-\frac{6\beta}{16\lambda m_2}\left(\frac{\sqrt{(\varepsilon^2-\kappa^2)\lambda} - \varepsilon\sqrt{\lambda}\cos\left(2\sqrt{\lambda}(\eta+h)\right)}{\varepsilon\sin\left(2\sqrt{\lambda}(\eta+h)\right)+\kappa}\right)^4 - \frac{6\beta\lambda}{16m}}{\left(\frac{\sqrt{(\varepsilon^2-\kappa^2)\lambda} - \varepsilon\sqrt{\lambda}\cos\left(2\sqrt{\lambda}(\eta+h)\right)}{\varepsilon\sin\left(2\sqrt{\lambda}(\eta+h)\right)+\kappa}\right)^2}, \tag{23}$$

$$u(\eta) = \frac{\beta}{4m} + \frac{-\frac{6\beta}{16\lambda m_2}\left(\frac{-\sqrt{(\varepsilon^2-\kappa^2)\lambda} - \varepsilon\sqrt{\lambda}\cos\left(2\sqrt{\lambda}(\eta+h)\right)}{\varepsilon\sin\left(2\sqrt{\lambda}(\eta+h)\right)+\kappa}\right)^4 - \frac{6\beta\lambda}{16m}}{\left(\frac{-\sqrt{(\varepsilon^2-\kappa^2)\lambda} - \varepsilon\sqrt{\lambda}\cos\left(2\sqrt{\lambda}(\eta+h)\right)}{\varepsilon\sin\left(2\sqrt{\lambda}(\eta+h)\right)+\kappa}\right)^2}, \tag{24}$$

$$u(\eta) = \frac{\beta}{4m} + \frac{-\frac{6\beta}{16\lambda m_2}\left(\mathrm{I}\sqrt{\lambda} - \frac{2\mathrm{I}\varepsilon\sqrt{\lambda}}{\varepsilon+\cos\left(2\sqrt{\lambda}(\eta+h)\right) - \mathrm{I}\sin\left(2\sqrt{\lambda}(\eta+h)\right)}\right)^4 - \frac{6\beta\lambda}{16m}}{\left(\mathrm{I}\sqrt{\lambda} - \frac{2\mathrm{I}\varepsilon\sqrt{\lambda}}{\varepsilon+\cos\left(2\sqrt{\lambda}(\eta+h)\right) - \mathrm{I}\sin\left(2\sqrt{\lambda}(\eta+h)\right)}\right)^2}, \tag{25}$$

$$u(\eta) = \frac{\beta}{4m} + \frac{-\frac{6\beta}{16\lambda m_2}\left(-\mathrm{I}\sqrt{\lambda} + \frac{2\varepsilon\sqrt{\lambda}}{\varepsilon+\cos\left(2\sqrt{\lambda}(\eta+h)\right) + \mathrm{I}\sin\left(2\sqrt{\lambda}(\eta+h)\right)}\right)^4 - \frac{6\beta\lambda}{16m}}{\left(-\mathrm{I}\sqrt{\lambda} + \frac{2\varepsilon\sqrt{\lambda}}{\varepsilon+\cos\left(2\sqrt{\lambda}(\eta+h)\right) + \mathrm{I}\sin\left(2\sqrt{\lambda}(\eta+h)\right)}\right)^2}, \tag{26}$$

where $\eta = kx - \sqrt{\frac{16k^2\alpha^2\lambda - \beta}{16\lambda}} \frac{\Gamma(n+1)}{p} t^p$.

For $\lambda < 0$, the hyperbolic solutions are

$$u(\eta) = \frac{\beta}{4m} + \frac{-\frac{6\beta}{16\lambda m_2}\left(\frac{\sqrt{-(\varepsilon^2+\kappa^2)\lambda} - \varepsilon\sqrt{-\lambda}\cosh\left(2\sqrt{-\lambda}(\eta+h)\right)}{\varepsilon\sinh\left(2\sqrt{-\lambda}(\eta+h)\right)+\kappa}\right)^4 - \frac{6\beta\lambda}{16m}}{\left(\frac{\sqrt{-(\varepsilon^2+\kappa^2)\lambda} - \varepsilon\sqrt{-\lambda}\cosh\left(2\sqrt{-\lambda}(\eta+h)\right)}{\varepsilon\sinh\left(2\sqrt{-\lambda}(\eta+h)\right)+\kappa}\right)^2}, \tag{27}$$

$$u(\eta) = \frac{\beta}{4m} + \frac{-\frac{6\beta}{16\lambda m_2}\left(\frac{-\sqrt{-(\varepsilon^2+\kappa^2)\lambda} - \varepsilon\sqrt{-\lambda}\cosh\left(2\sqrt{-\lambda}(\eta+h)\right)}{\varepsilon\sinh\left(2\sqrt{-\lambda}(\eta+h)\right)+\kappa}\right)^4 - \frac{6\beta\lambda}{16m}}{\left(\frac{-\sqrt{-(\varepsilon^2+\kappa^2)\lambda} - \varepsilon\sqrt{-\lambda}\cosh\left(2\sqrt{-\lambda}(\eta+h)\right)}{\varepsilon\sinh\left(2\sqrt{-\lambda}(\eta+h)\right)+\kappa}\right)^2}, \tag{28}$$

$$u(\eta) = \frac{\beta}{4m} + \frac{-\frac{6\beta}{16\lambda m_2}\left(\sqrt{-\lambda} - \frac{2\varepsilon\sqrt{-\lambda}}{\varepsilon+\cosh\left(2\sqrt{-\lambda}(\eta+h)\right) - \sinh\left(2\sqrt{-\lambda}(\eta+h)\right)}\right)^4 - \frac{6\beta\lambda}{16m}}{\left(\sqrt{-\lambda} - \frac{2\varepsilon\sqrt{-\lambda}}{\varepsilon+\cosh\left(2\sqrt{-\lambda}(\eta+h)\right) - \sinh\left(2\sqrt{-\lambda}(\eta+h)\right)}\right)^2}, \tag{29}$$

$$u(\eta)=\frac{\beta}{4m}+\frac{-\frac{6\beta}{16\lambda m_2}\left(-\sqrt{-\lambda}+\frac{2\varepsilon\sqrt{-\lambda}}{\varepsilon+\cosh\left(2\sqrt{-\lambda}(\eta+h)\right)+\sinh\left(2\sqrt{-\lambda}(\eta+h)\right)}\right)^4-\frac{6\beta\lambda}{16m}}{\left(-\sqrt{-\lambda}+\frac{2\varepsilon\sqrt{-\lambda}}{\varepsilon+\cosh\left(2\sqrt{-\lambda}(\eta+h)\right)+\sinh\left(2\sqrt{-\lambda}(\eta+h)\right)}\right)^2}, \tag{30}$$

where $\eta=kx-\sqrt{\frac{16k^2\alpha^2\lambda-\beta}{16\lambda}}\frac{\Gamma(n+1)}{p}t^p$.

Case 02: $=\sqrt{\frac{4k^2\alpha^2\lambda+\beta}{4\lambda}}, p_0=\frac{3\beta}{2m}, q_2=p_1=0, p_2=\frac{6\beta}{4m\lambda}$, $q_3=0$.

For $\lambda>0$, the trigonometric solutions are

$$u(\eta)=\frac{3\beta}{2m}+\frac{6\beta}{4m\lambda}\left(\frac{\sqrt{(\varepsilon^2-\kappa^2)\lambda}-\varepsilon\sqrt{\lambda}\cos\left(2\sqrt{\lambda}(\eta+h)\right)}{\varepsilon\sin\left(2\sqrt{\lambda}(\eta+h)\right)+\kappa}\right)^2, \tag{31}$$

$$u(\eta)=\frac{3\beta}{2m}+\frac{6\beta}{4m\lambda}\left(\frac{-\sqrt{(\varepsilon^2-\kappa^2)\lambda}-\varepsilon\sqrt{\lambda}\cos\left(2\sqrt{\lambda}(\eta+h)\right)}{\varepsilon\sin\left(2\sqrt{\lambda}(\eta+h)\right)+\kappa}\right)^2, \tag{32}$$

$$u(\eta)=\frac{3\beta}{2m}+\frac{6\beta}{4m\lambda}\left(\mathrm{I}\sqrt{\lambda}-\frac{2I\varepsilon\sqrt{\lambda}}{\varepsilon+\cos\left(2\sqrt{\lambda}(\eta+h)\right)-\mathrm{I}\sin\left(2\sqrt{\lambda}(\eta+h)\right)}\right)^2, \tag{33}$$

$$u(\eta)=\frac{3\beta}{2m}+\frac{6\beta}{4m\lambda}\left(-\mathrm{I}\sqrt{\lambda}+\frac{2\varepsilon\sqrt{\lambda}}{\varepsilon+\cos\left(2\sqrt{\lambda}(\eta+h)\right)+\mathrm{I}\sin\left(2\sqrt{\lambda}(\eta+h)\right)}\right)^2, \tag{34}$$

where $\eta=kx-\sqrt{\frac{4k^2\alpha^2\lambda+\beta}{4\lambda}}\frac{\Gamma(n+1)}{p}t^p$.

For $\lambda<0$, the hyperbolic solutions are

$$u(\eta)=\frac{3\beta}{2m}+\frac{6\beta}{4m\lambda}\left(\frac{\sqrt{-(\varepsilon^2+\kappa^2)\lambda}-\varepsilon\sqrt{-\lambda}\cosh\left(2\sqrt{-\lambda}(\eta+h)\right)}{\varepsilon\sinh\left(2\sqrt{-\lambda}(\eta+h)\right)+\kappa}\right)^2, \tag{35}$$

$$u(\eta)=\frac{3\beta}{2m}+\frac{6\beta}{4m\lambda}\left(\frac{-\sqrt{-(\varepsilon^2+\kappa^2)\lambda}-\varepsilon\sqrt{-\lambda}\cosh\left(2\sqrt{-\lambda}(\eta+h)\right)}{\varepsilon\sinh\left(2\sqrt{-\lambda}(\eta+h)\right)+\kappa}\right)^2, \tag{36}$$

$$u(\eta)=\frac{3\beta}{2m}+\frac{6\beta}{4m\lambda}\left(\sqrt{-\lambda}-\frac{2\varepsilon\sqrt{-\lambda}}{\varepsilon+\cosh\left(2\sqrt{-\lambda}(\eta+h)\right)-\sinh\left(2\sqrt{-\lambda}(\eta+h)\right)}\right)^2, \tag{37}$$

$$u(\eta)=\frac{3\beta}{2m}+\frac{6\beta}{4m\lambda}\left(-\sqrt{-\lambda}+\frac{2\varepsilon\sqrt{-\lambda}}{\varepsilon+\cosh\left(2\sqrt{-\lambda}(\eta+h)\right)+\sinh\left(2\sqrt{-\lambda}(\eta+h)\right)}\right)^2, \tag{38}$$

where $\eta = kx - \sqrt{\frac{4k^2\alpha^2\lambda+\beta}{4\lambda}}\frac{\Gamma(n+1)}{p}t^p$.

Case 03: $k = \frac{1}{\alpha}\sqrt{\frac{16\lambda w^2+\beta}{16\lambda}}, p_0 = \frac{1}{4}\frac{\beta}{m}, p_1 = 0, p_2 = -\frac{3}{8}\frac{\beta}{\lambda m}$, $q_2 = 0, q_3 = -\frac{3}{8}\frac{\beta\lambda}{m}$.

For $\lambda > 0$, the trigonometric solutions are

$$u(\eta) = \frac{\beta}{4m} - \frac{-\frac{3}{8}\frac{\beta}{\lambda m}\left(\frac{\sqrt{(\varepsilon^2-\kappa^2)\lambda}-\varepsilon\sqrt{\lambda}\cos\left(2\sqrt{\lambda}(\eta+h)\right)}{\varepsilon\sin\left(2\sqrt{\lambda}(\eta+h)\right)+\kappa}\right)^4 + \frac{3}{8}\frac{\beta\lambda}{m}}{\left(\frac{\sqrt{(\varepsilon^2-\kappa^2)\lambda}-\varepsilon\sqrt{\lambda}\cos\left(2\sqrt{\lambda}(\eta+h)\right)}{\varepsilon\sin\left(2\sqrt{\lambda}(\eta+h)\right)+\kappa}\right)^2}, \tag{39}$$

$$u(\eta) = \frac{\beta}{4m} - \frac{-\frac{3}{8}\frac{\beta}{\lambda m}\left(\frac{-\sqrt{(\varepsilon^2-\kappa^2)\lambda}-\varepsilon\sqrt{\lambda}\cos\left(2\sqrt{\lambda}(\eta+h)\right)}{\varepsilon\sin\left(2\sqrt{\lambda}(\eta+h)\right)+\kappa}\right)^4 + \frac{3}{8}\frac{\beta\lambda}{m}}{\left(\frac{-\sqrt{(\varepsilon^2-\kappa^2)\lambda}-\varepsilon\sqrt{\lambda}\cos\left(2\sqrt{\lambda}(\eta+h)\right)}{\varepsilon\sin\left(2\sqrt{\lambda}(\eta+h)\right)+\kappa}\right)^2}, \tag{40}$$

$$u(\eta) = \frac{\beta}{4m} - \frac{-\frac{3}{8}\frac{\beta}{\lambda m}\left(\mathrm{I}\sqrt{\lambda} - \frac{2\mathrm{I}\varepsilon\sqrt{\lambda}}{\varepsilon+\cos\left(2\sqrt{\lambda}(\eta+h)\right)-\mathrm{I}\sin\left(2\sqrt{\lambda}(\eta+h)\right)}\right)^4 + \frac{3}{8}\frac{\beta\lambda}{m}}{\left(\mathrm{I}\sqrt{\lambda} - \frac{2\mathrm{I}\varepsilon\sqrt{\lambda}}{\varepsilon+\cos\left(2\sqrt{\lambda}(\eta+h)\right)-\mathrm{I}\sin\left(2\sqrt{\lambda}(\eta+h)\right)}\right)^2}, \tag{41}$$

$$u(\eta) = \frac{\beta}{4m} - \frac{-\frac{3}{8}\frac{\beta}{\lambda m}\left(-\mathrm{I}\sqrt{\lambda} + \frac{2\varepsilon\sqrt{\lambda}}{\varepsilon+\cos\left(2\sqrt{\lambda}(\eta+h)\right)+\mathrm{I}\sin\left(2\sqrt{\lambda}(\eta+h)\right)}\right)^4 + \frac{3}{8}\frac{\beta\lambda}{m}}{\left(-\mathrm{I}\sqrt{\lambda} + \frac{2\varepsilon\sqrt{\lambda}}{\varepsilon+\cos\left(2\sqrt{\lambda}(\eta+h)\right)+\mathrm{I}\sin\left(2\sqrt{\lambda}(\eta+h)\right)}\right)^2}, \tag{42}$$

where $\eta = \frac{1}{\alpha}\sqrt{\frac{16\lambda w^2+\beta}{16\lambda}}x - \omega\frac{\Gamma(n+1)}{p}t^p$.

For $\lambda > 0$, the hyperbolic solutions are

$$u(\eta) = \frac{\beta}{4m} - \frac{-\frac{3}{8}\frac{\beta}{\lambda m}\left(\frac{\sqrt{-(\varepsilon^2+\kappa^2)\lambda}-\varepsilon\sqrt{-\lambda}\cosh\left(2\sqrt{-\lambda}(\eta+h)\right)}{\varepsilon\sinh\left(2\sqrt{-\lambda}(\eta+h)\right)+\kappa}\right)^4 + \frac{3}{8}\frac{\beta\lambda}{m}}{\left(\frac{\sqrt{-(\varepsilon^2+\kappa^2)\lambda}-\varepsilon\sqrt{-\lambda}\cosh\left(2\sqrt{-\lambda}(\eta+h)\right)}{\varepsilon\sinh\left(2\sqrt{-\lambda}(\eta+h)\right)+\kappa}\right)^2}, \tag{43}$$

$$u(\eta) = \frac{\beta}{4m} - \frac{-\frac{3}{8}\frac{\beta}{\lambda m}\left(\frac{-\sqrt{-(\varepsilon^2+\kappa^2)\lambda}-\varepsilon\sqrt{-\lambda}\cosh\left(2\sqrt{-\lambda}(\eta+h)\right)}{\varepsilon\sinh\left(2\sqrt{-\lambda}(\eta+h)\right)+\kappa}\right)^4 + \frac{3}{8}\frac{\beta\lambda}{m}}{\left(\frac{-\sqrt{-(\varepsilon^2+\kappa^2)\lambda}-\varepsilon\sqrt{-\lambda}\cosh\left(2\sqrt{-\lambda}(\eta+h)\right)}{\varepsilon\sinh\left(2\sqrt{-\lambda}(\eta+h)\right)+\kappa}\right)^2}, \tag{44}$$

$$u(\eta) = \frac{\beta}{4m} - \frac{-\frac{3}{8}\frac{\beta}{\lambda m}\left(\sqrt{-\lambda} - \frac{2\varepsilon\sqrt{-\lambda}}{\varepsilon+\cosh\left(2\sqrt{-\lambda}(\eta+h)\right)-\sinh\left(2\sqrt{-\lambda}(\eta+h)\right)}\right)^4 + \frac{3}{8}\frac{\beta\lambda}{m}}{\left(\sqrt{-\lambda} - \frac{2\varepsilon\sqrt{-\lambda}}{\varepsilon+\cosh\left(2\sqrt{-\lambda}(\eta+h)\right)-\sinh\left(2\sqrt{-\lambda}(\eta+h)\right)}\right)^2}, \tag{45}$$

$$u(\eta) = \frac{\beta}{4m} - \frac{-\frac{3}{8}\frac{\beta}{\lambda m}\left(-\sqrt{-\lambda} + \frac{2\varepsilon\sqrt{-\lambda}}{\varepsilon+\cosh\left(2\sqrt{-\lambda}(\eta+h)\right)+\sinh\left(2\sqrt{-\lambda}(\eta+h)\right)}\right)^4 + \frac{3}{8}\frac{\beta\lambda}{m}}{\left(-\sqrt{-\lambda} + \frac{2\varepsilon\sqrt{-\lambda}}{\varepsilon+\cosh\left(2\sqrt{-\lambda}(\eta+h)\right)+\sinh\left(2\sqrt{-\lambda}(\eta+h)\right)}\right)^2}, \tag{46}$$

where $\eta = \frac{1}{\alpha}\sqrt{\frac{16\lambda w^2+\beta}{16\lambda}}x - \omega\frac{\Gamma(n+1)}{p}t^p$.

3.3. Application of Advanced $\exp(-\phi(\eta))$*-Expansion Method.* Consider the solution of Equation (21) as follows:

$$u(\xi) = a_0 + a_1 e^{-F(\eta)} + a_2 e^{-F(\eta)2}. \tag{47}$$

According to the tanh method, inserting Equation (31) with Equation (16) into Equation (21), we get the following system of equations.

$e^{4F(\eta)}: (-2\alpha^2k^2a_1\theta_1\theta_2 + 2w^2a_1\theta_1\theta_2 - 2ma_0a_1 + \beta a_1) = 0,$
$e^{3F(\eta)}: (-8\alpha^2k^2a_2\theta_1\theta_2 + 8w^2a_2\theta_1\theta_2 - 2ma_0a_2 - ma_1^2 + \beta a_2) = 0,$
$e^{2F(\eta)}: (-2\alpha^2k^2a_1\theta_1^2 + 2w^2a_1\theta_1^2 - 2ma_1a_2) = 0,$
$e^{F(\eta)}: -6\alpha^2k^2a_2\theta_1^2 + 6w^2a_2\theta_1^2 - ma_2^2 = 0,$
$e^{F(\eta)0}: -2\alpha^2k^2a_2\theta_2^2 + 2w^2a_2\theta_2^2 - ma_0^2 + \beta a_0 = 0.$

After using Maple to solve the aforementioned system of equations, the following four sets of solutions will be obtained.

Case 01: $k = \frac{1}{\alpha}\sqrt{\frac{-4w^2\theta_1\theta_2-\beta}{-4\theta_1\theta_2}}, w = w, a_0 = -\frac{1}{2}\frac{\beta}{m}, a_1 = 0$, $a_2 = -\frac{3}{2}\frac{\beta\theta_1}{\theta_2 m}$.

For $\theta_1\theta_2 > 0$, the trigonometric solutions are

$$u(\eta) = -\frac{1}{2}\frac{\beta}{m} - \frac{3}{2}\frac{\beta\theta_1}{\theta_2 m}\left(\sqrt{\frac{\theta_1}{\theta_2}}\tan\left(\sqrt{\theta_1\theta_2}(\eta+h)\right)\right)^2, \tag{48}$$

$$u(\eta)=-\frac{1}{2}\frac{\beta}{m}-\frac{3}{2}\frac{\beta\theta_1}{\theta_2 m}\left(\sqrt{\frac{\theta_1}{\theta_2}}\cot\left(\sqrt{\theta_1\theta_2}(\eta+h)\right)\right)^2, \tag{49}$$

where $\eta=\frac{1}{\alpha}\sqrt{\frac{-4w^2\theta_1\theta_2-\beta}{-4\theta_1\theta_2}}x-w\frac{\Gamma(n+1)}{p}t^p$.

For $\theta_1\theta_2<0$, the hyperbolic solutions are

$$u(\eta)=-\frac{1}{2}\frac{\beta}{m}-\frac{3}{2}\frac{\beta\theta_1}{\theta_2 m}\left(\sqrt{\frac{\theta_1}{-\theta_2}}\tanh\left(\sqrt{-\theta_1\theta_2}(\eta+h)\right)\right)^2, \tag{50}$$

$$u(\eta)=-\frac{1}{2}\frac{\beta}{m}-\frac{3}{2}\frac{\beta\theta_1}{\theta_2 m}\left(\sqrt{\frac{\theta_1}{-\theta_2}}\coth\left(\sqrt{-\theta_1\theta_2}(\eta+h)\right)\right)^2, \tag{51}$$

where $\eta=\frac{1}{\alpha}\sqrt{\frac{-4w^2\theta_1\theta_2-\beta}{-4\theta_1\theta_2}}x-w\frac{\Gamma(n+1)}{p}t^p$.

When $\theta_2>0$ and $\theta_1=0$ and $\theta_2=0$ and $\theta_1\in\mathbb{R}$, the solution is rejected.

Case 02: $k=k, w=\frac{1}{\alpha}\sqrt{\frac{-4k^2\theta_1\theta_2+\beta}{-4\theta_1\theta_2}}, a_0=-\frac{1}{2}\frac{\beta}{m}, a_1=0$, $a_2=-\frac{3}{2}\frac{\beta\theta_1}{\theta_2 m}$.

For $\theta_1\theta_2>0$, the trigonometric solutions are

$$u(\eta)=-\frac{1}{2}\frac{\beta}{m}-\frac{3}{2}\frac{\beta\theta_1}{\theta_2 m}\left(\sqrt{\frac{\theta_1}{\theta_2}}\tan\left(\sqrt{\theta_1\theta_2}(\eta+h)\right)\right)^2, \tag{52}$$

$$u(\eta)=-\frac{1}{2}\frac{\beta}{m}-\frac{3}{2}\frac{\beta\theta_1}{\theta_2 m}\left(\sqrt{\frac{\theta_1}{\theta_2}}\cot\left(\sqrt{\theta_1\theta_2}(\eta+h)\right)\right)^2, \tag{53}$$

where $\eta=\mathrm{k}x-\frac{1}{\alpha}\sqrt{\frac{-4k^2\alpha^2\theta_1\theta_2+\beta}{-4\theta_1\theta_2}}\frac{\Gamma(n+1)}{p}t^p$.

For $\theta_1\theta_2<0$, the hyperbolic solutions are

$$u(\eta)=-\frac{1}{2}\frac{\beta}{m}-\frac{3}{2}\frac{\beta\theta_1}{\theta_2 m}\left(\sqrt{\frac{\theta_1}{-\theta_2}}\tanh\left(\sqrt{-\theta_1\theta_2}(\eta+h)\right)\right)^2, \tag{54}$$

$$u(\eta)=-\frac{1}{2}\frac{\beta}{m}-\frac{3}{2}\frac{\beta\theta_1}{\theta_2 m}\left(\sqrt{\frac{\theta_1}{-\theta_2}}\coth\left(\sqrt{-\theta_1\theta_2}(\eta+h)\right)\right)^2, \tag{55}$$

where $\eta=\mathrm{k}x-\frac{1}{\alpha}\sqrt{\frac{-4k^2\alpha^2\theta_1\theta_2+\beta}{-4\theta_1\theta_2}}\frac{\Gamma(n+1)}{p}t^p$.

When $\theta_2>0$ and $\theta_1=0$, the solution is rejected.

When $\theta_2=0$ and $\theta_1\in\mathbb{R}$, the solution is rejected.

4. Graphical Comparison of β-Fraction Derivative and M-Fraction Derivative Solutions

Solitary wave solutions of nonlinear evolution equations are significant as they represent localized, self-reinforcing waves that maintain their shape and speed during propagation. They are useful in many disciplines, including biology, oceanography, and physics. Comprehending solitary waves aids in forecasting and managing wave behavior, investigating phenomena such as soliton interactions, and creating effective communication networks and material conveyance systems. Furthermore, isolated waves are essential components in the study of emergent phenomena and nonlinear dynamics in complex systems. We discuss the geometric solution of the obtained fractional K-G problem solution in this section. The analytical answers that are derived can be used to determine the direction, speed, and frequency of electromagnetic waves as well as their propagation in a particular medium. We investigate several wave patterns via Maple 18 for the free parameter values and also show how the fractional derivative affects the wave pattern that is constructed with various 2D and 3D density graphs. In this section, using graphical representations, we show and discuss the obtained analytical solutions provided by Equations (23), (24), (25), (26), (27), (28), (29), (30), (31), (32), (33), (34), (35), (36), (37), (38), (39), (40), (41), (42), (43), (44), (45), (46), (47), (48), (49), (50), (51), (52), (53), (54), and (55). These solutions originate from the K-G model with β-derivative and M-truncated derivatives, and their physical explanations depend on the parameters that were selected for the underlying model. For the selected parameters $p=0.5$, we compared the β-derivative and the M-truncated derivative. We include graphical outputs of some soliton solutions in Figures 1, 2, 3, 4, 5, 6, 7, 8, 9, and 10 to observe the shape and behavior of the obtained analytical solutions such as various periodic waves, lumps with cross-periodic waves, periodic rogue waves, unique soliton, bright bell shapes, dark bell shapes, kink shapes, and other shapes.

4.1. Unified Technique. In this subdivision, the unified technique is applied to the fractional K-G equation. The generated solutions are expressed as trigonometric, hyperbolic, and rational function forms. To understand the dynamics inherent in the results, it is necessary to grasp the physical elucidation of the obtained solutions. In this portion, we determine the visual illustrations of the solutions we have evolved, operating the three-dimensional with density plots and two-dimensional plots to reveal our obvious solutions. By using the unified technique, we plot some profile of the periodic wave, lump with cross periodic wave, periodic rogue wave, singular soliton wave, etc. These profiles find extensive applications in fields like as nonlinear optics, plasma physics, and fuzzy dynamics.

In Figure 1, the solution (Equation (23)) provided the periodic wave solutions for $\alpha=-0.1, \beta=-1, m=2, k=\frac{1}{2}$, $\lambda=\frac{1}{5}$, $\varepsilon=4, \kappa=\frac{1}{5}$, $h=-0.001$, $\theta=\frac{3}{2}$, and $p=0.5$. Here, Figures 1(a) and 1(c) show the 3D plot of β-fractional effect; Figures 1(b) and 1(d) show the 3D plot of M-fractional effect; and Figure 1(e) shows the 2D plot of the comparative

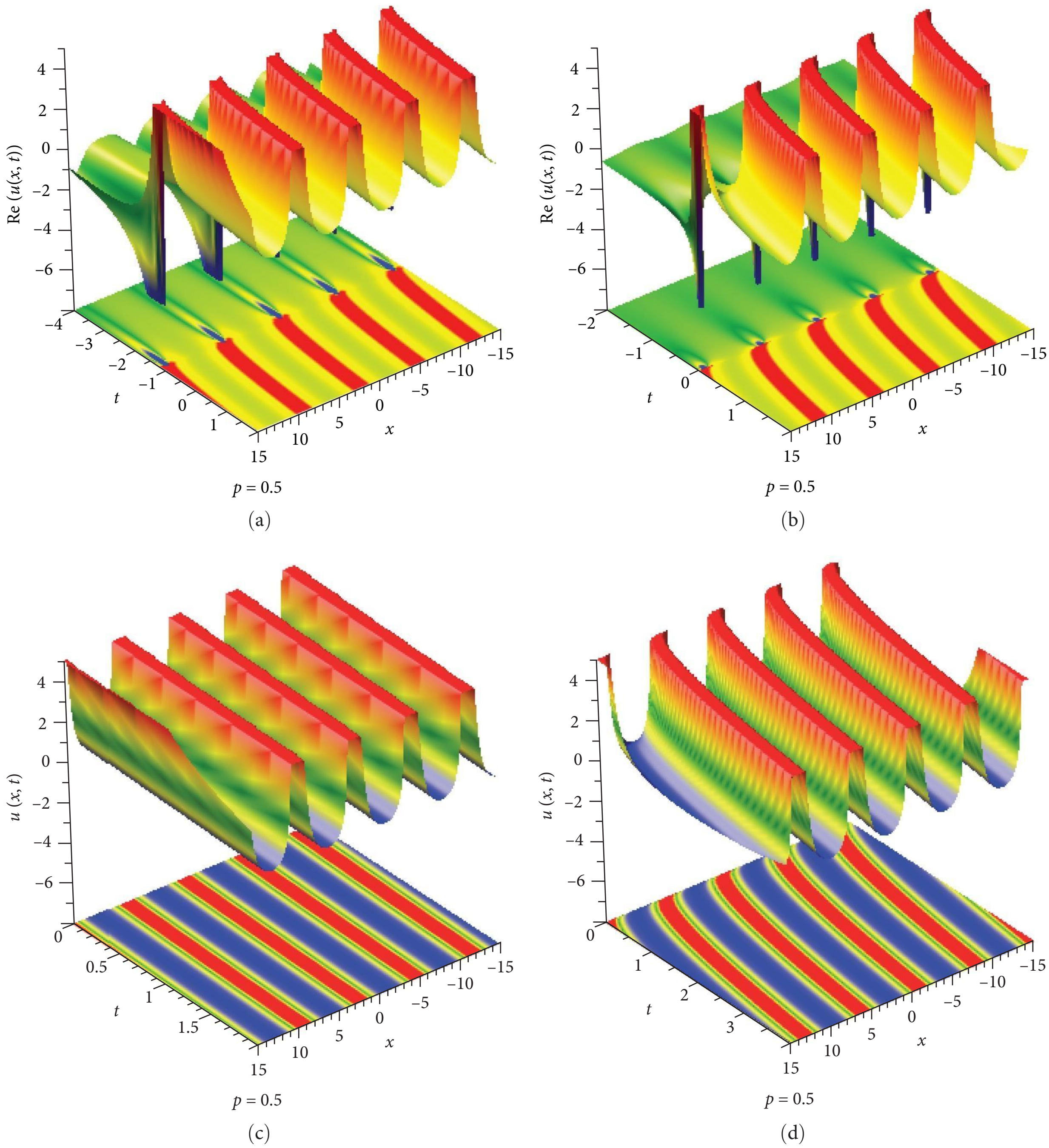

Figure 1: Continued.

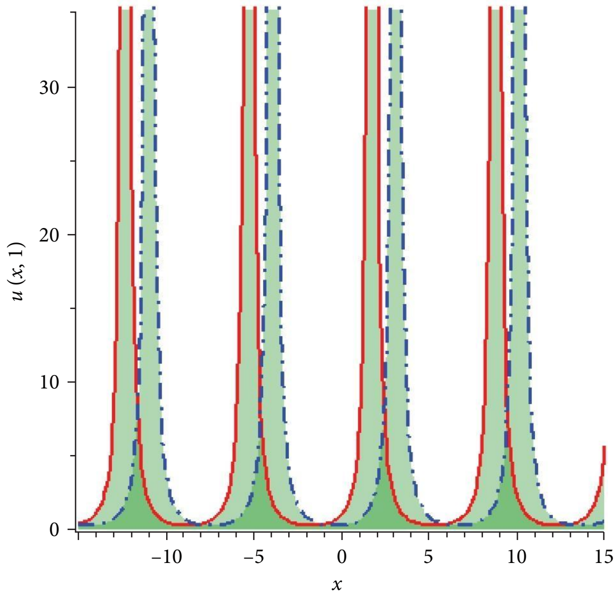

(e)

Figure 1: Feature of the solution (Equation (23)): (a) and (c) show the 3D plot of the β-fractional effect; (b) and (d) show the 3D plot of the M-fractional effect; and (e) shows the comparative effect 2D plots between them.

effect of these fractions. Feature of the lump with cross-periodic wave solutions of Equation (26) for $\alpha=1$, $\beta=1.3$, $m=1$, $k=0.1$, $\lambda=\frac{1}{5}$, $\varepsilon=-1.6, \kappa:=1.5$, $h=\frac{1}{100}$, $\theta=\frac{3}{2}$, and $p=0.5$ illustrated in Figure 2. Here, Figures 2(a) and 2(c) show the 3D plot of β-fractional effect; Figures 2(b) and 2(d) display the 3D plot of M-fractional effect; and Figures 2(e), 2(f), 2(g), and 2(h) show the appearance of the 2D plot of the comparative effect of these fractions. In Figure 3, the solution (Equation (31)) illustrates the periodic rogue wave solutions for $\alpha=1$, $\beta=-1$, $m=1$, $\omega=\frac{1}{3}$, $\lambda=\frac{1}{5}$, $\varepsilon=1.6, \kappa=1.5$, $h=-1$, $n=\frac{3}{2}$, and $p=0.9$. Here Figure 3(a) shows the 3D plot of β-fractional effect; Figure 3(b) shows the 3D plot of M-fractional effect; and Figures 3(c) and 3(d) show the comparative effect 2D plots between the β-fraction and M-fraction. In Figure 4, the solutions in Equation (35) illustrated singular soliton for $\alpha=1$, $\beta=-2$, $m=1$, $\omega=1$, $\lambda=-\frac{1}{2}$, $\varepsilon=1, \kappa=1.5$, $h=-1, n=\frac{3}{2}$, and $p=0.5$; Figure 4(a) displays the 3D diagram of β-fractional effect; Figure 4(b) shows the demonstrations of the 3D diagram of M-fractional effect; and Figure 4(c) shows the demonstrations of the comparative effect 2D diagram between the β-fraction and M-fraction.

4.2. Advanced $\exp(-\phi(\xi))$*-Expansion Method.* In this subdivision, the advanced $\exp(-\phi(\xi))$-expansion technique is applied to the fractional K-G equation. The generated solutions are expressed as trigonometric, hyperbolic, and rational function forms. To understand the dynamics inherent in the results, it is necessary to grasp the physical elucidation of the obtained solutions. In this portion, we determine the visual illustrations of the solutions we have evolved, operating the three-dimensional with density plots and two-dimensional plots to reveal our obvious solutions. By using the advanced $\exp(-\phi(\xi))$-expansion technique, we plot some profiles of periodic waves, bright bell shapes, dark bell shapes, antikink shape waves, kink shape waves, etc. These profiles find extensive applications in fields like as nonlinear optics, plasma physics, and fuzzy dynamics.

In Figure 5, the feature of the periodic wave is illustrated from the solution in Equation (48) for $\alpha=-1, \beta=1, m=5$, $\omega=0.5$, $\lambda=-\frac{1}{2}$, $\theta_1=1.6$, $\theta_2=1.5$, $h=-1$, $n=\frac{3}{2}$, and $p=0.5$. Here, Figures 5(a) displays the 3D diagram of the effect of β-fraction; Figure 5(b) displays the 3D diagram of the effect of M-fraction; and Figure 5(c) demonstrates the 2D diagram of the comparative effect between the β-fraction and M-fraction. The solutions in Equation (51) provided the feature of bright bell shape solution for $\alpha=-1$, $\beta=1$, $m=-5, \omega=-1$, $\theta_1=-1.6$, $\theta_2=1.5$, $h=-1$, $n=\frac{3}{2}$, and $p=0.5$ illustrated in Figure 6. Here, Figure 6(a) demonstrates the 3D diagram of the effect of β-fraction; Figure 6(b) demonstrates the 3D diagram of the effect of M-fraction; and Figure 6(c) demonstrates the 2D plots of a comparative effect between the β-fraction and M-fraction. In Figure 7, the feature of dark bell shape solution of the Equation (51) illustrated for $\alpha=-1$, $\beta=1$, $\omega=-1$, $m=5$, $\theta_1=-1.6$, $\theta_2=1.5$, $h=-1$, $n=\frac{3}{2}$, and $p=0.5$; Figure 7(a) demonstrates the 3D diagram of the effect of β-fraction; Figure 7(b) demonstrates the 3D diagram of the effect of M-fractional effect; and Figure 7(c) shows the 2D diagram of a comparative study between the β-fraction and M-fraction. In Figure 8, the solution in Equation (53) provided the antikink wave solution with periodic wave for $\alpha=-1$, $m=-1$, $\beta=8$, $k=0.1$, $\theta_1=1.6$, $\theta_2=5$, $h=-1$, $n=\frac{3}{2}$, and $p=0.5$;

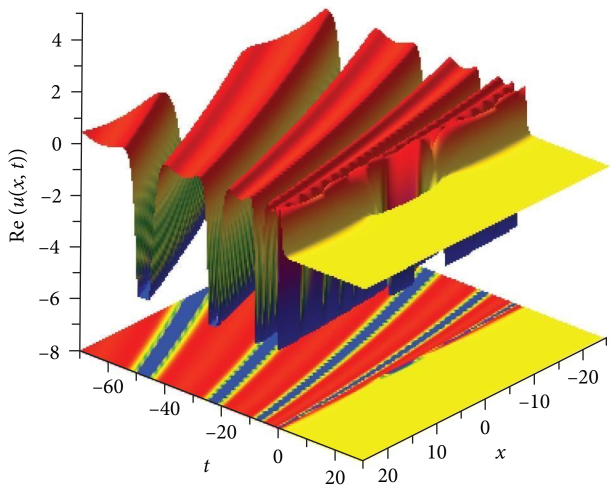

$p = 0.5$

(a)

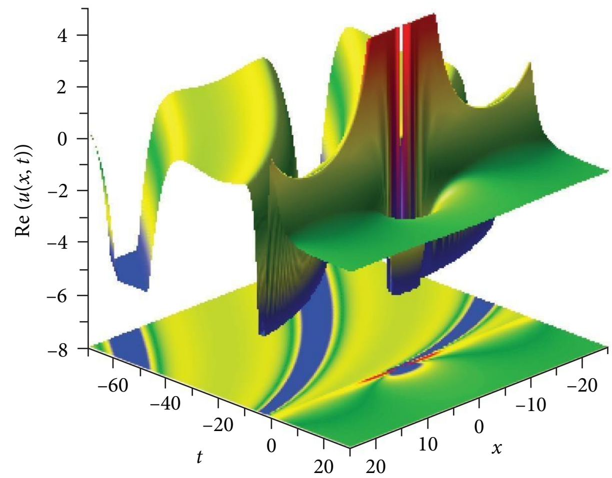

$p = 0.5$

(b)

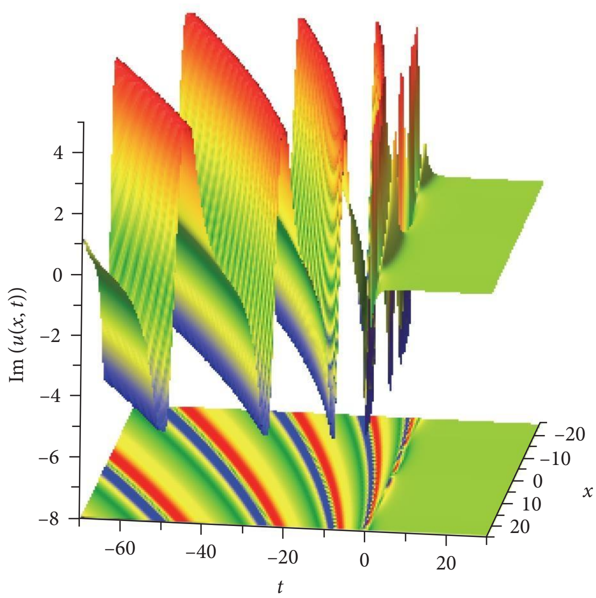

$p = 0.5$

(c)

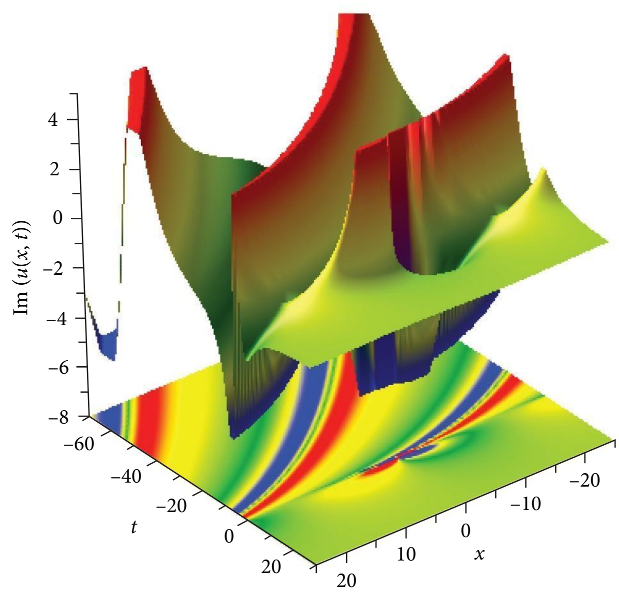

$p = 0.5$

(d)

Figure 2: Continued.

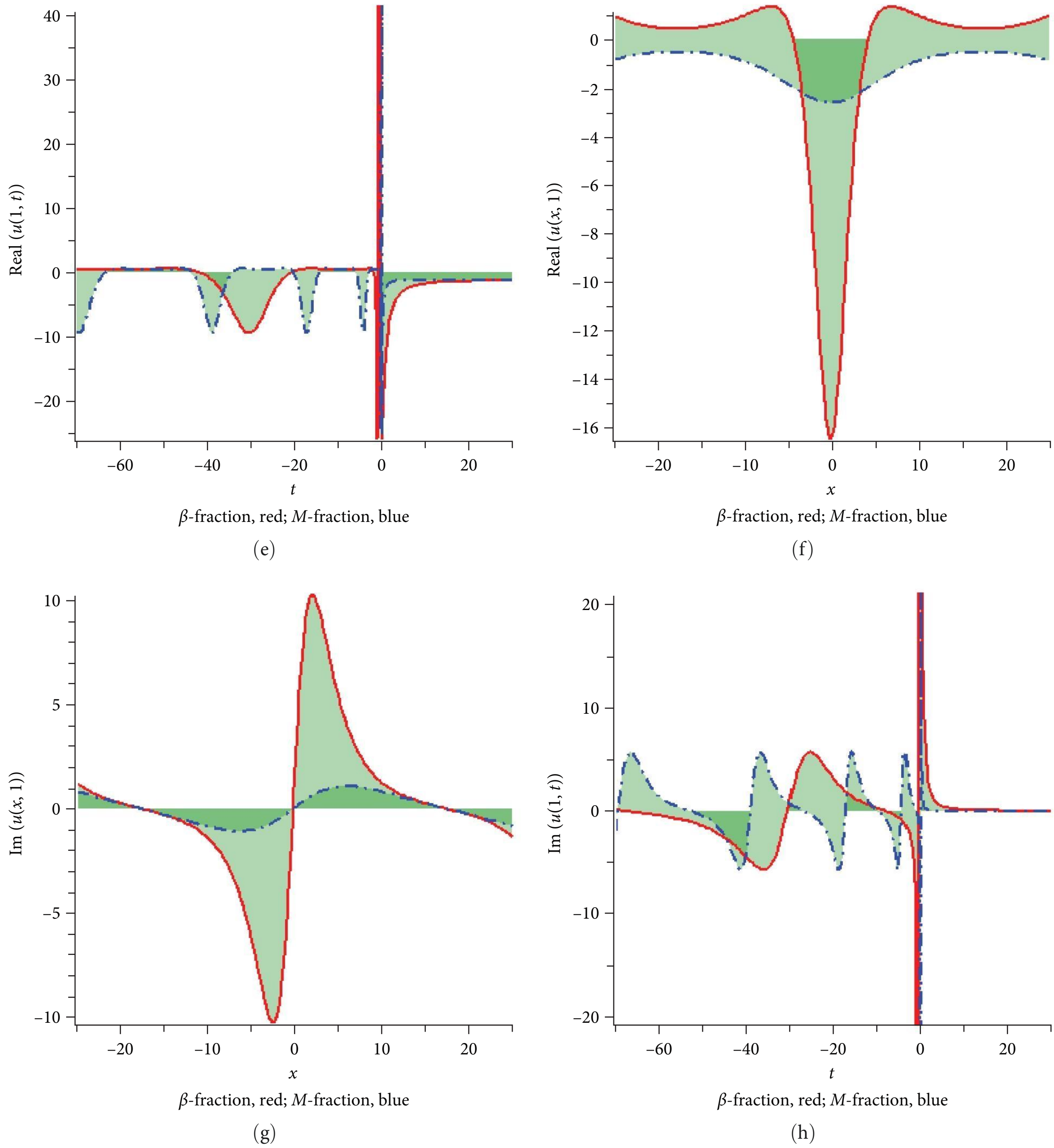

FIGURE 2: Feature of the solution (Equation (26)): (a) and (c) show the 3D plot of the β-fractional effect; (b) and (d) show the 3D plot of the M-fractional effect; and (e), (f), (g), and (h) show the comparative effect 2D plots between the above fraction.

Figure 8(a) demonstrates the 3D diagram of the effect of β-fractional effect; Figure 8(b) displays the 3D diagram of the effect of M-fractional effect; and Figure 8(c) displays the 2D diagram of the comparative effect between the β-fraction and M-fraction. In Figure 9, the feature of kink wave solution with the periodic wave of Equation (53) illustrates for $\alpha = -1$, $\beta = 8$, $m = 1$, $k = 0.1$, $\theta_1 = 1.6$, $\theta_2 = 5$, $h = -1$, $n = \frac{3}{2}$, and $p = 0.5$; Figure 9(a) displays the 3D diagram of the effect of β-fractional effect; Figure 9(b) displays the 3D diagram of the effect of M-fractional effect; and Figure 9(c) displays the 2D diagram of the comparative effect between the β-fraction and M-fraction. In Figure 10, the solution (Equation (53)) provided the periodic wave solution for $\alpha = -1$, $\beta = 8$, $k = 0.1$, $m = 1$, $\theta_1 = 1.6$, $\theta_2 = 5$, $h = -1$, $n = \frac{3}{2}$, and $p = 0.5$. Here,

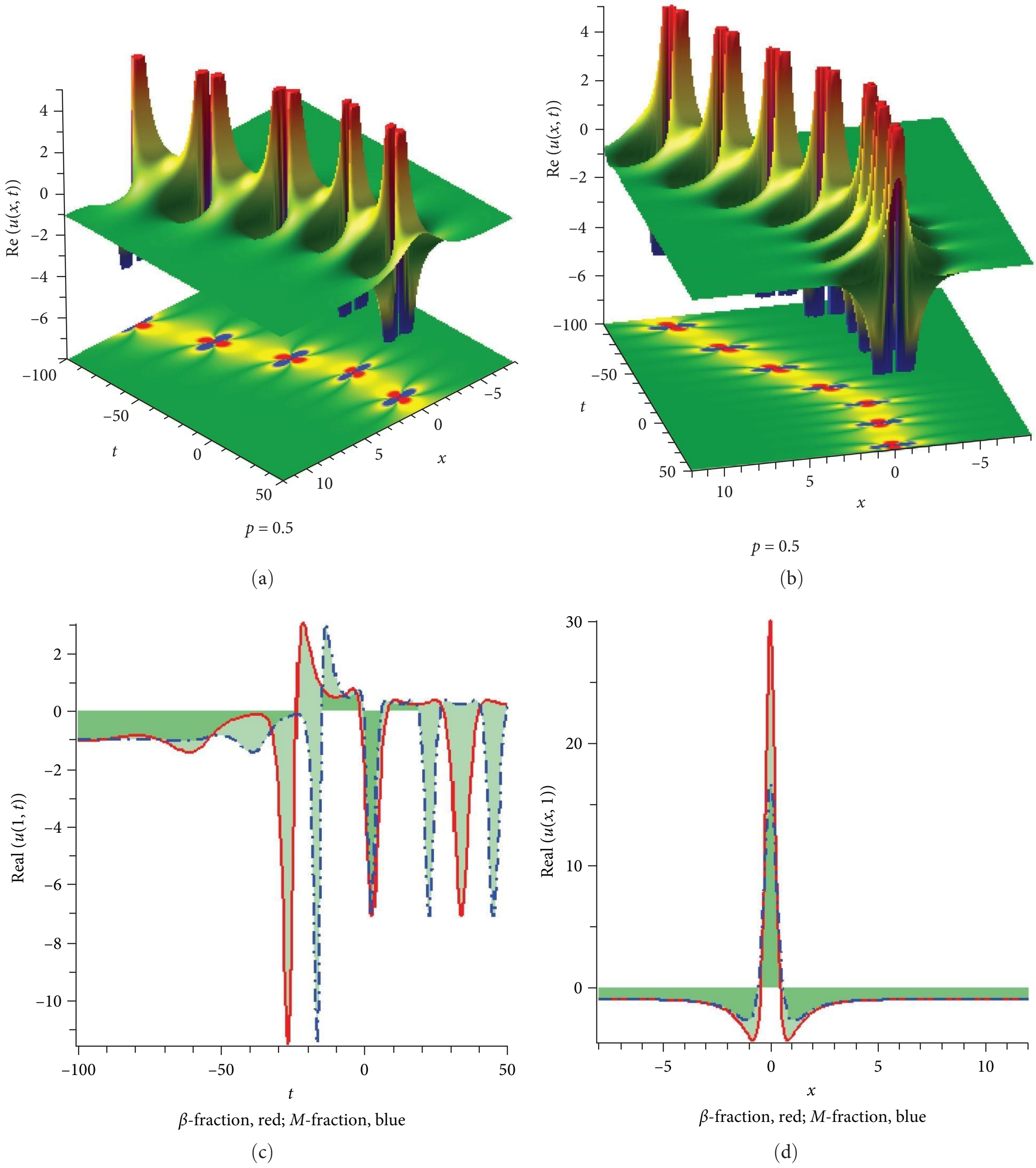

Figure 3: Feature of the solution (Equation (31)): (a) demonstrations of the 3D diagram of the effect of the β-fractional parameter; (b) demonstrations of the 3D diagram of the effect of M-fractional; and (c) and (d) display the comparative effect 2D plots between the β-fraction and M-fraction.

Figure 10(a) displays the 3D diagram of the effect of β-fractional effect; Figure 10(b) demonstrates the 3D diagram of the effect of M-fractional effect; and Figures 10(c) and 10(d) demonstrate the 2D diagram of the comparative effect between the β-fraction and M-fraction.

5. Comparison and Novelty

It is important to note that the two approaches we utilized here are relatively straightforward, easy to use, and need less computing power than the other approaches [57, 59].

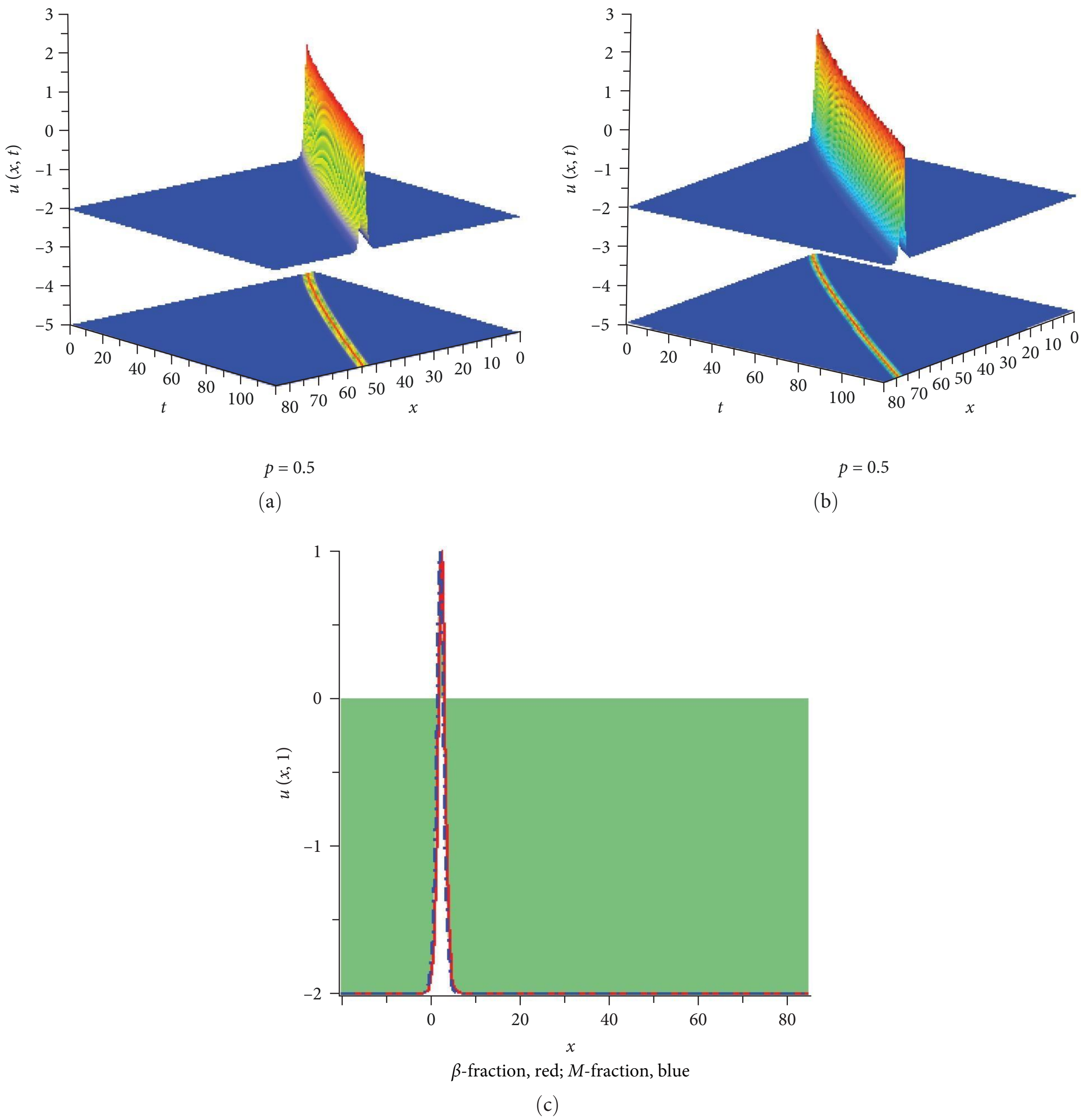

Figure 4: Feature of the solution (Equation (35)): (a) demonstrations of the 3D diagram of the β-fractional effect; (b) displays the 3D diagram of the M-fractional effect; and (c) demonstrations of the comparative effect between the β-fraction and M-fraction.

Additionally, these approaches can be employed without the usage of an auxiliary equation to show the underlying workings of the model. With the use of the auxiliary equation, Sirendaoreji [57] was able to solve the quadratic nonlinear K-G model using the auxiliary approach and extract the solitary, periodic, and unique solutions in real form. In addition, Zhang [59] used the exp-function approach to solve the same model and extract a few solutions, which included solitary and periodic waves solely in real form. However, all of their solutions were covered by our answers, which were derived using the two approaches and found to be solitary, periodic, and unique in both real and complex forms. We retrieved many resolutions of the KG model that were not described in [57, 59], including diverse bounded and unbounded periodic waves, dark and brilliant bell shapes, dark-bright and bright-dark kink waves, polynomial solutions, disguised versions of soliton, and periodic rouge waves.

6. Modulation Instability

In a nonlinear model, the stability of a solution can be found in a relation between nonlinear and dispersive terms. In

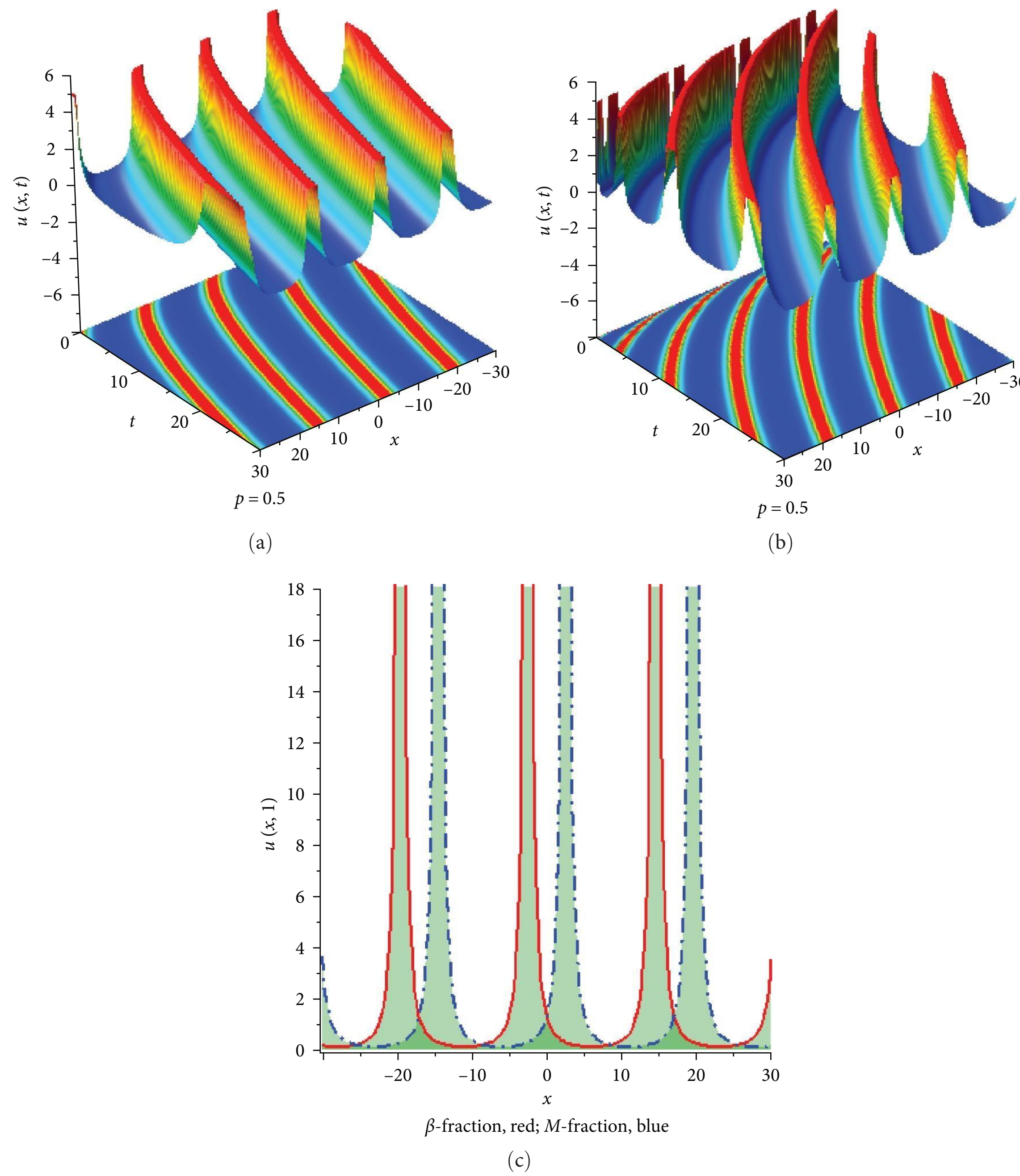

Figure 5: Feature of the solution (Equation (48)): (a) displays the 3D plot of the β-fractional effect; (b) displays the 3D plot of the M-fractional effect; and (c) demonstrations of the comparative effect 2D plots between the β-fraction and M-fraction.

general, for the fiber communication model to meet the stable solution of the nonlinear model, there will be instability caused by the collision of the nonlinear component with the dispersive term, which is known as modulation instability. As a result, small disturbances superimposed on a plane wave grow exponentially. The regulation of diverse nonlinear models or events is based on the research of modulation instability areas, which is applied in many fields.

In this section, we explore the modulation instability of traveling waves of the K-G model in the following form:

$$L_{tt} - \alpha^2 L_{xx} + \beta L - mL^2 = 0. \tag{56}$$

We will perform a modulation instability analysis [67], which involves looking for perturbed solutions of the form:

$$L(x, t) = \wp + \mathscr{E} P(x, t). \tag{57}$$

Here, $P(x, t)$ is the slowly varying envelope.

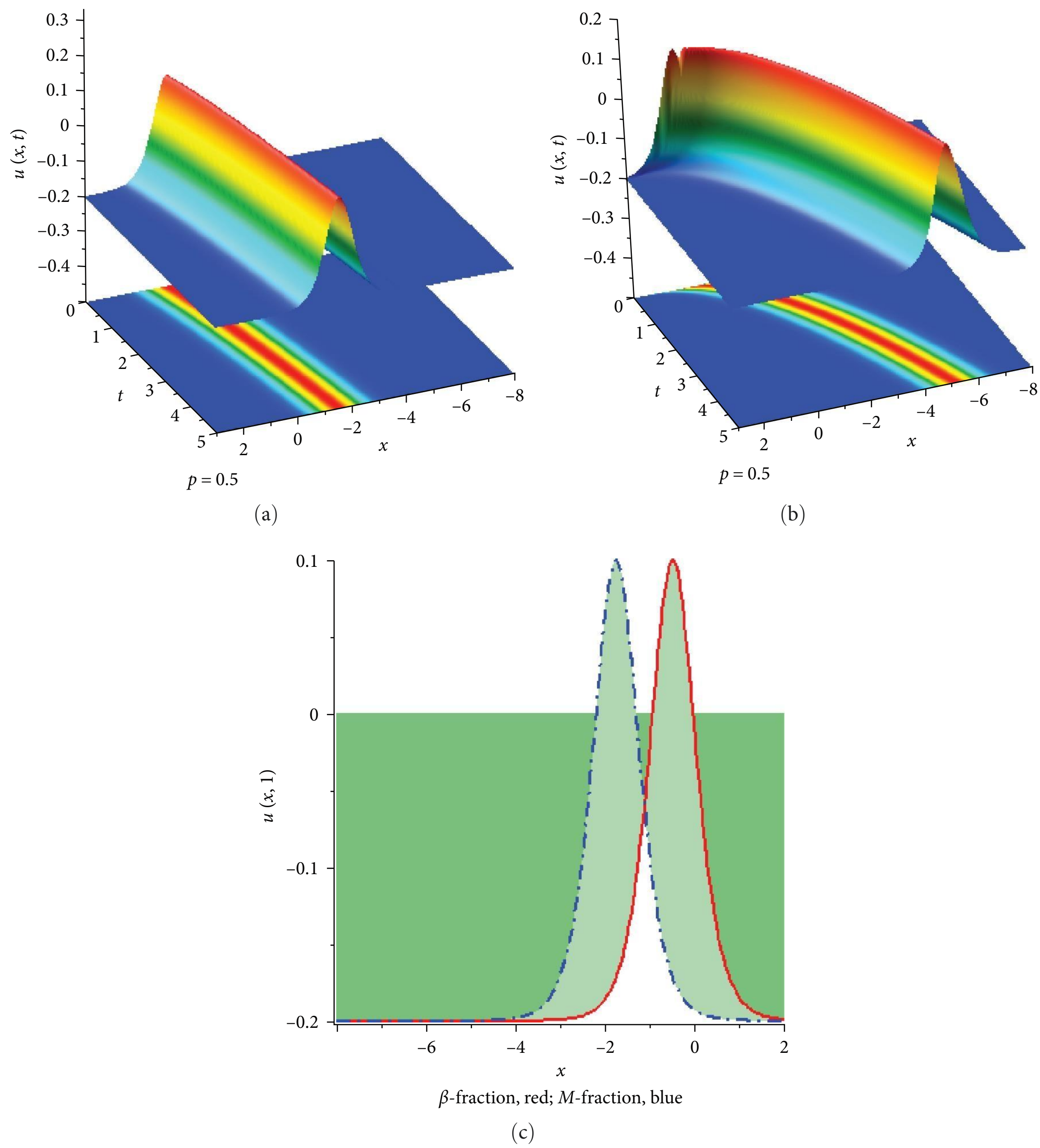

FIGURE 6: Feature of the solution (Equation (51)) for $m<0$: (a) displays the 3D plot of the β-fractional effect; (b) displays the 3D plot of the M-fractional effect; and (c) demonstrations of the comparative effect 2D plots between the β-fraction and M-fraction.

Substituting Equation (57) into Equation (56), then we get

$$\mathscr{E}P_{tt} - \mathscr{E}\alpha^2 P_{xx} + \beta(\wp + \mathscr{E}P(x,t)) - m(\wp + \mathscr{E}P(x,t))^2 = 0, \tag{58}$$

and linearizing in $\mathscr{E}$,

$$\mathscr{E}P_{tt}(x,t) - \mathscr{E}\alpha^2 P_{xx}(x,t) + \beta\mathscr{E}P(x,t) - 2m\wp\mathscr{E}P(x,t) = 0. \tag{59}$$

Let us consider the solution of Equation (58) as

$$P(x,t) = e^{i(kx-\omega t)}. \tag{60}$$

Here, k is the wave number, and ω is the angular frequency.

Substituting Equation (60) into Equation (58) and dividing the entire equation by $e^{i(kx-\omega t)}$, then we get $\mathscr{E}\omega^2 - \mathscr{E}\alpha^2 k^2 + \beta\mathscr{E} - 2m\wp\mathscr{E} = 0$.

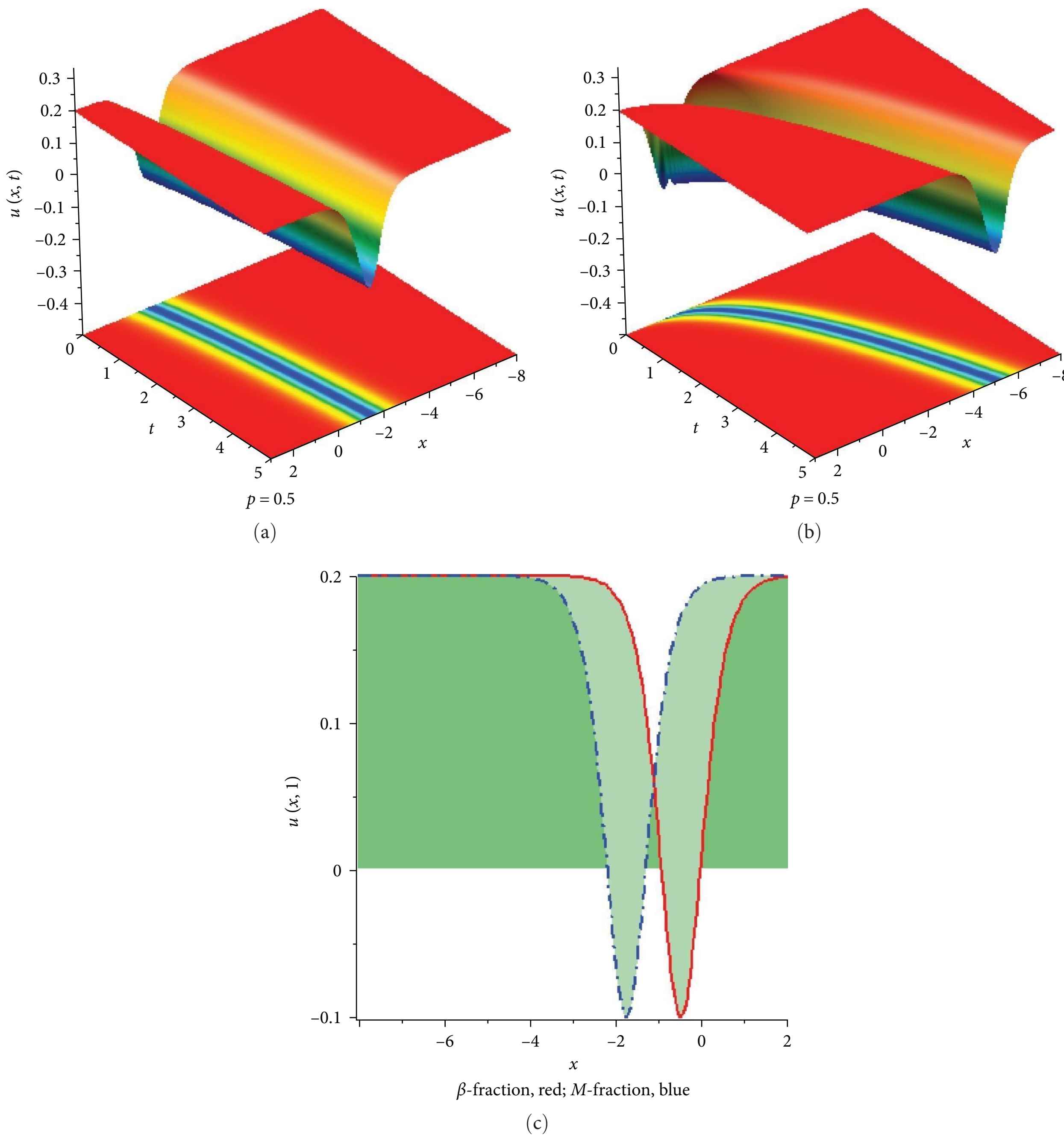

FIGURE 7: Feature of the solution (Equation (51)) for $m>0$: (a) displays the 3D plot of the β-fractional effect; (b) displays the 3D plot of the M-fractional effect; and (c) demonstrations of the comparative effect 2D plots between the β-fraction and M-fraction.

The dispersion relation is given by the following equation:

$$\omega = \pm\sqrt{\alpha^2 k^2 - \beta + 2m\wp}. \tag{61}$$

It can be written as

$$g(\omega) = 2lm(\omega) = 2lm\left(\sqrt{\alpha^2 k^2 - \beta + 2m\wp}\right). \tag{62}$$

In Figure 11, modulation instability spectrum is illustrated utilizing a linear analysis technique.

Solitary wave solutions of nonlinear evolution equations are significant as they represent localized, self-reinforcing waves that maintain their shape and speed during propagation. They are useful in many disciplines, including biology, oceanography, and physics. In this work, we have successfully implemented the unified and advanced $\exp(-\phi(\eta))$-expansion techniques to explore the exact solitary solutions

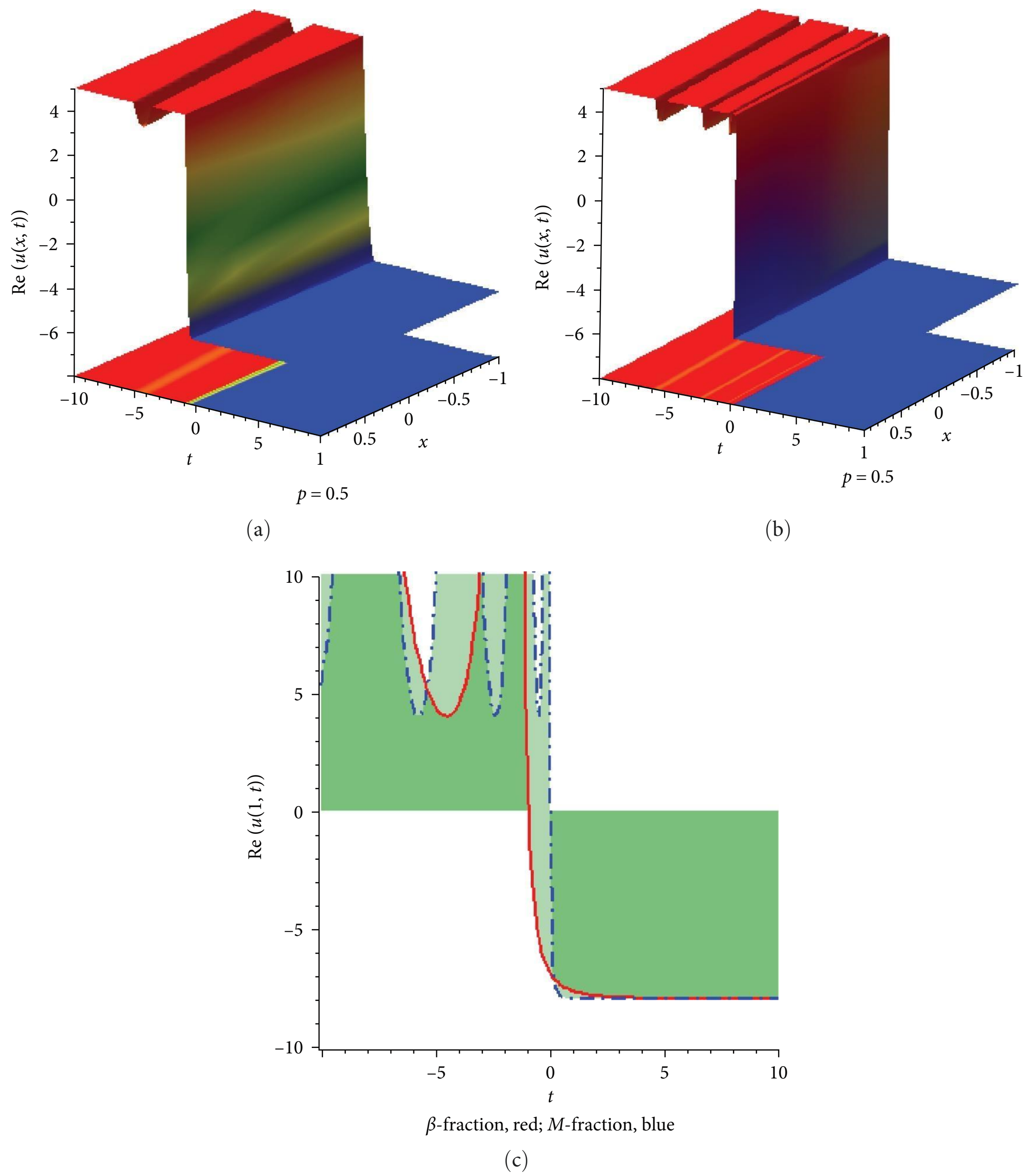

FIGURE 8: Feature of the solution (Equation (53)) for $m<0$: (a) displays the 3D plot of the β-fractional effect; (b) displays the 3D plot of the M-fractional effect; and (c) demonstrations of the comparative effect 2D plots between the β-fraction and M-fraction.

from the time-fractional Klien-Gordon model. To solve the fractional version of Klein–Gordon, we engaged β-fractional and M-truncated fractional derivatives. The obtained analytical solutions are presented in trigonometric, hyperbolic functions, and rational function forms. For the special value of the parameters, we plotted some significant wave patterns with 3D, density, and 2D graph form such as periodic waves, lumps with cross-periodic waves, periodic rogue waves, singular waves by unified technique, and periodic waves, bright bells, dark bells, kinks, antikinks, and periodic wave behaviors by advanced $\exp(-\phi(\eta))$-expansion technique. We compared the fractional effects between the β-derivative and M-fractional derivatives and illustrated through graphs (2D) by assigning particular values to fractional parameters. However, from the explanations and implementations, we concluded that the M-fractional derivative is more effective than the β-fractional derivative. Additionally, the modulation instability spectrum can be expressed utilizing a linear analysis technique, and the modulation instability bands are shown to be influenced by the third-order dispersion term.

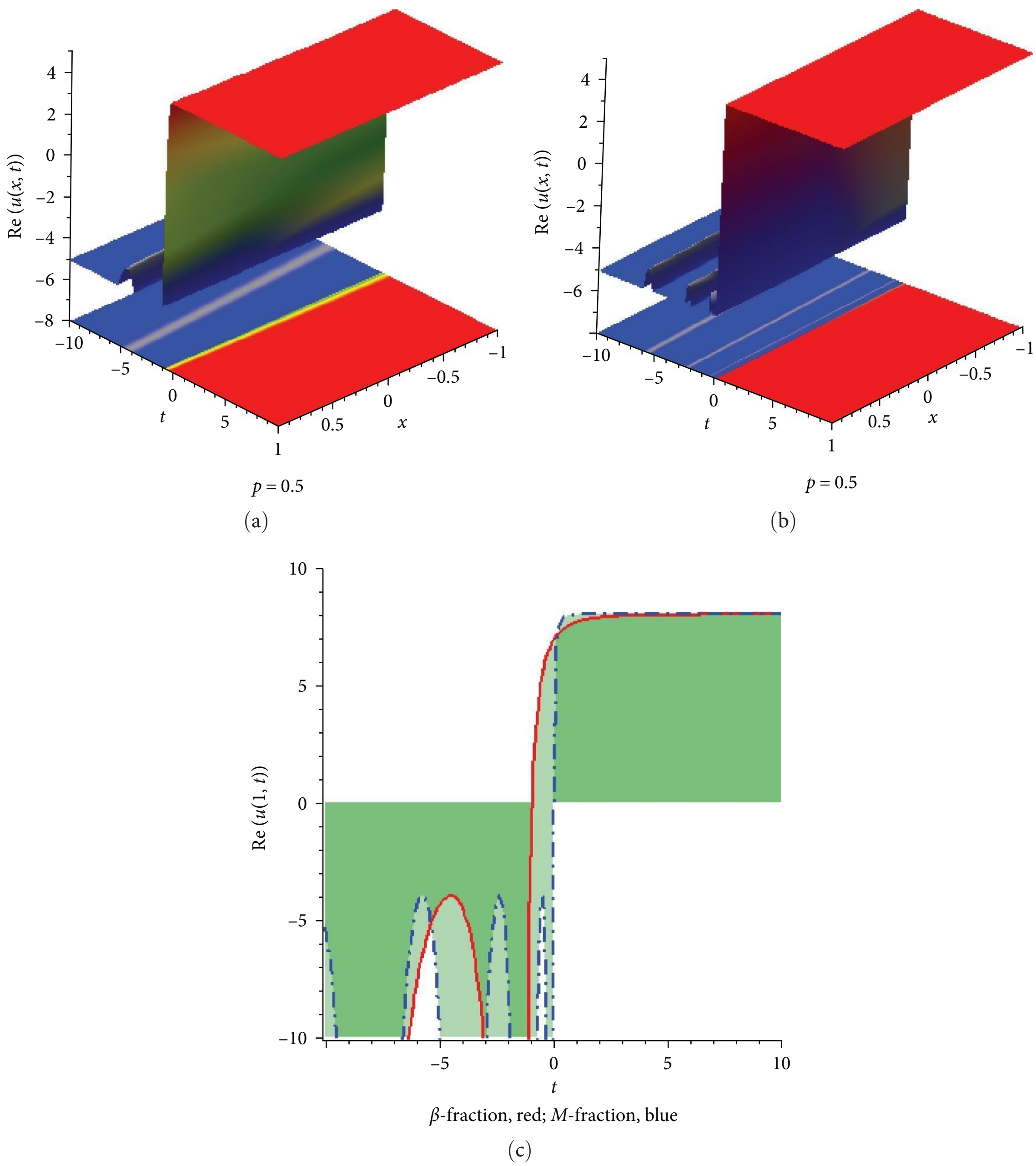

Figure 9: Feature of the solution (Equation (53)) for $m > 0$: (a) displays the 3D plot of the β-fractional effect; (b) displays the 3D plot of the M-fractional effect; and (c) demonstrations of the comparative effect 2D plots between the β-fraction and M-fraction.

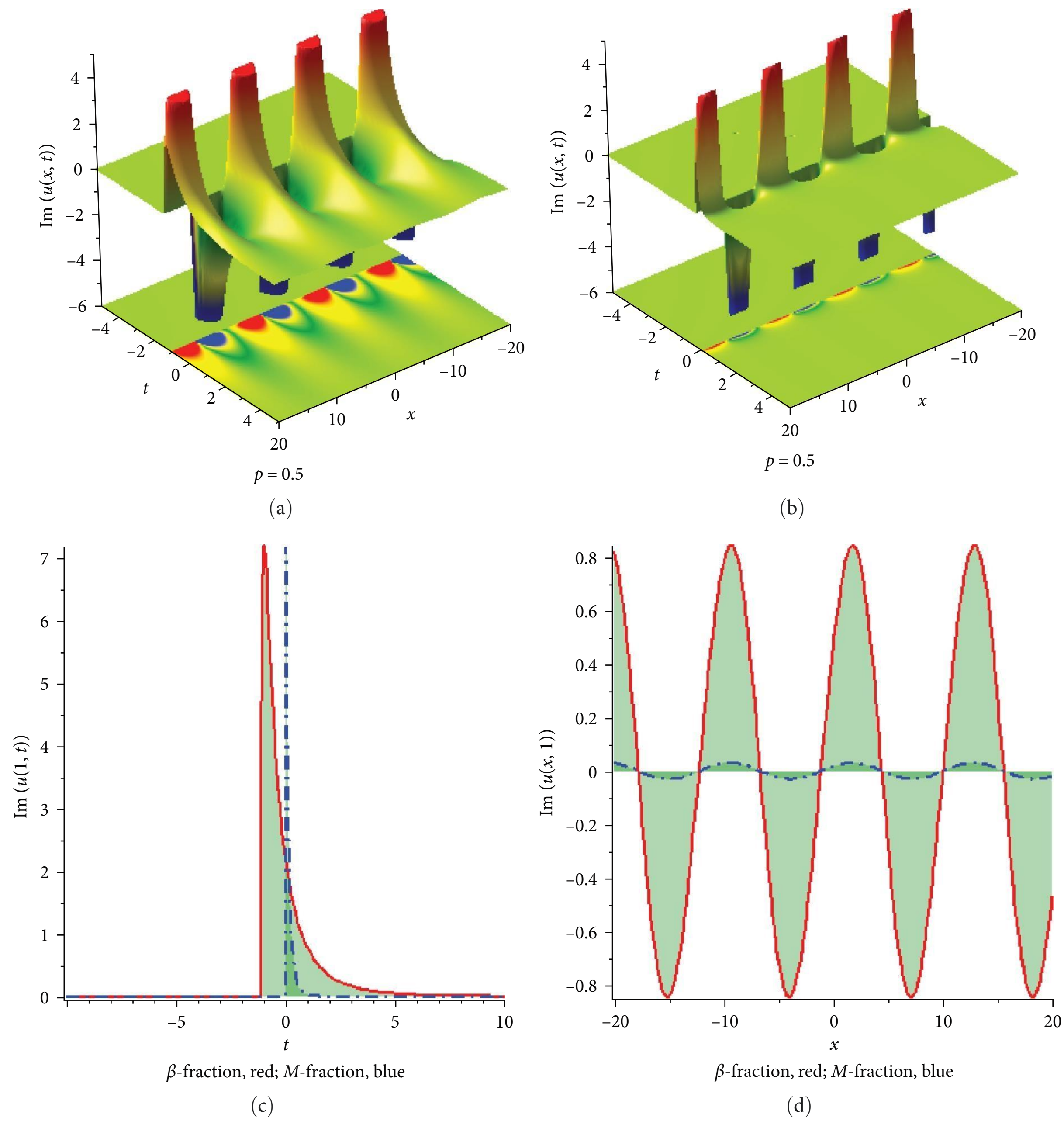

FIGURE 10: Feature of the solution (Equation (53)): (a) displays the 3D plot of the β-fractional effect; (b) displays the 3D plot of the M-fractional effect; (c) and (d) demonstrate the comparative effect 2D plots between the β-fraction and M-fraction.

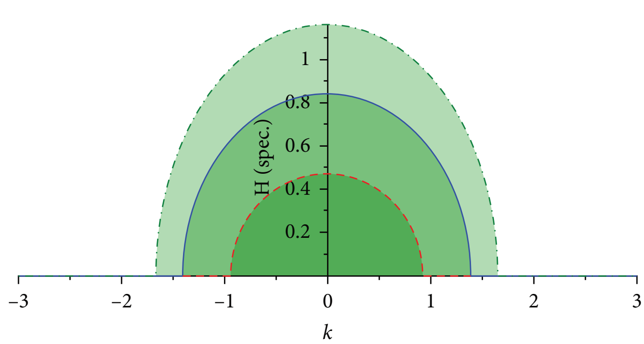

FIGURE 11: Gain spectrum of MI for different values of $\alpha = [0.5, 0.6, 0.7]$, $\beta = [0.1, 0.3, 0.5]$, $m = [-0.2, -0.4, -0.6]$, $\wp = [0.3, 0.5, 0.7]$.

The performance results of the examined wave are reliable for the researchers and have significant implications for mathematics and optical physics.

Data Availability

The simulation data used to support the findings of this study are available from the corresponding author upon request.

Conflicts of Interest

The authors declare that they have no known competing interests for this work.

Authors' Contributions

Md. Mamunur Roshid conceptualized this work, wrote the codes, generated the figures, and wrote the main manuscript. Mosfiqur Rahman updated the codes, analyzed the figures, and modified the manuscript. Mahtab Uddin configured the methodology, investigated this work, modified the figures, and finalized the manuscript. Harun Or-Roshid supervised the work, checked the results, and modified the manuscript.

References

[1] M. S. Islam, M. M. Roshid, A. K. M. L. Rahman, and M. A. Akbar, "Solitary wave solutions in plasma physics and acoustic gravity waves of some nonlinear evolution equations through enhanced MSE method," *Journal of Physics Communications*, vol. 3, no. 12, Article ID 125011, 2019.

[2] H. M. Baskonus, H. Bulut, and T. A. Sulaiman, "New complex hyperbolic structures to the lonngren-wave equation by using sine-Gordon expansion method," *Applied Mathematics and Nonlinear Sciences*, vol. 4, no. 1, pp. 129–138, 2019.

[3] M. Jia, "Soliton molecules and few-cycle-pulse solitons structures for the generalized Konopelchenko-Dubrovsky–Kaup-Kupershmidt equation," *Nonlinear Dynamics*, vol. 111, pp. 19359–19369, 2023.

[4] S. Ur Rehman, J. Ahmad, and T. Muhammad, "Dynamics of novel exact soliton solutions to Stochastic Chiral Nonlinear Schrödinger equation," *Engineering Journal*, vol. 79, pp. 568–580, 2023.

[5] M. M. Roshid, A. Abdeljabbar, A. Aldurayhim, M. M. Rahman, Harun-Or-Roshid, and F. S. Alshammari, "Dynamical interaction of solitary, periodic, rogue type wave solutions and multi-soliton solutions of the nonlinear models," *Heliyon*, vol. 8, no. 12, Article ID e11996, 2022.

[6] S. Hossain, M. M. Roshid, M. Uddin, A. A. Ripa, and H.-O. Roshid, "Abundant time-wavering solutions of a modified regularized long wave model using the EMSE technique," *Partial Differential Equations in Applied Mathematics*, vol. 8, Article ID 100551, 2023.

[7] J. J. Yang, S. F. Tian, and Z. Q. Li, "Inverse scattering problem for the matrix modified Korteweg–de Vries equation with finite density type initial data," *Physica D: Nonlinear Phenomena*, vol. 455, Article ID 133911, 2023.

[8] W. B. Rabie and H. M. Ahmed, "Optical solitons for multiple-core couplers with polynomial law of nonlinearity using the modified extended direct algebraic method," *Optik*, vol. 258, Article ID 168848, 2022.

[9] A. Houwe, S. Abbagari, L. Akinyemi, Y. Saliou, M. Justin, and S. Y. Doka, "Modulation instability, bifurcation analysis and solitonic waves in nonlinear optical media with odd-order dispersion," *Physics Letters A*, vol. 488, Article ID 129134, 2023.

[10] K. K. Ali, A. M. Wazwaz, and M. S. Osman, "Optical soliton solutions to the generalized nonautonomous nonlinear Schrödinger equations in optical fibers via the sine-Gordon expansion method," *Optik*, vol. 208, Article ID 164132, 2020.

[11] M. Arshad, D. Lu, and J. Wang, "(N+ 1)-dimensional fractional reduced differential transform method for fractional order partial differential equations," vol. 48, pp. 509–519, Communications in Nonlinear Science and Numerical Simulation, 2017.

[12] M. A. Umer, M. Arshad, A. R. Seadawy, I. Ahmed, and M. Tanveer, "Exploration conversations laws, different rational solitons and vibrant type breather wave solutions of the modify unstable nonlinear Schrödinger equation with stability and its multidisciplinary applications," *Optical and Quantum Electronics*, vol. 56, no. 3, Article ID 420, 2024.

[13] A. Sarwar, T. Gang, M. Arshad, and I. Ahmed, "Construction of bright-dark solitary waves and elliptic function solutions of space-time fractional partial differential equations and their applications," *Physica Scripta*, vol. 95, no. 4, Article ID 045227, 2020.

[14] M. Rudolph-Lilith, "A discrete algebraic framework for stochastic systems which yield unique and exact solutions," *Heliyon*, vol. 4, no. 7, Article ID e00691, 2018.

[15] J. Dvornik, A. J. Lazarevic, D. Lazarevic, and M. Uros, "Exact arithmetic as a tool for convergence assessment of the IRM-CG method," *Heliyon*, vol. 6, no. 1, Article ID e03225, 2020.

[16] W.-X. Ma and J.-H. Lee, "A transformed rational function method and exact solutions to the $3+1$ dimensional Jimbo–Miwa equation," *Chaos, Solitons & Fractals*, vol. 42, no. 3, pp. 1356–1363, 2009.

[17] Y. J. Yang, "The fractional residual method for solving the local fractional differential equations," *Thermal Science*, vol. 24, no. 4, pp. 2535–2542, 2020.

[18] S. O. Akindeinde, "A new multistage technique for approximate analytical solution of nonlinear differential equations," *Heliyon*, vol. 6, no. 10, Article ID e05188, 2020.

[19] L. Ali, S. Islam, T. Gul, M. A. Khan, and E. Bonyah, "Solutions of nonlinear real world problems by a new analytical technique," *Heliyon*, vol. 4, no. 11, Article ID e00913, 2018.

[20] U. Younas, F. Yao, N. Nasreen, A. Khan, and T. Abdeljawad, "Dynamics of M-truncated optical solitons and other solutions to the fractional Kudryashov's equation," *Results in Physics*, vol. 58, Article ID 107503, 2024.

[21] M. A. Arefin, M. A. Saeed, M. A. Akbar, and M. H. Uddin, "Analytical behavior of weakly dispersive surface and internal waves in the ocean," *Journal of Ocean Engineering and Science*, vol. 7, no. 4, pp. 305–312, 2022.

[22] A. Podder, M. A. Arefin, M. A. Akbar, and M. H. Uddin, "A study of the wave dynamics of the space–time fractional nonlinear evolution equations of beta derivative using the improved Bernoulli sub-equation function approach," *Scientific Reports*, vol. 13, no. 1, Article ID 20478, 2023.

[23] M. A. Arefin, M. A. Khatun, M. S. Islam, M. A. Akbar, and M. H. Uddin, "Explicit soliton solutions to the fractional order nonlinear models through the atangana beta derivative," *International Journal of Theoretical Physics*, vol. 62, no. 6, Article ID 134, 2023.

[24] J. Cen, F. Correa, and A. Fring, "Degenerate multi-solitons in the sine-Gordon equation," *Journal of Physics A: Mathematical and Theoretical*, vol. 50, no. 43, Article ID 435201, 2017.

[25] E. M. E. Zayed, R. M. A. Shohib, M. E. M. Alngar et al., "Solitons and conservation laws in magneto-optic waveguides with generalized Kudryashov's equation by the unified auxiliary equation approach," *Optik*, vol. 245, Article ID 167694, 2021.

[26] Y. Du, T. Yin, and J. Pang, "The exact solutions of Schrödinger–Hirota equation based on the auxiliary equation method," *Optical and Quantum Electronics*, vol. 56, no. 5, Article ID 712, 2024.

[27] G. C. Paul, F. Z. Eti, and D. Kumar, "Dynamical analysis of lump, lump-triangular periodic, predictable rogue and breather wave solutions to the (3+1)-dimensional gKP-Boussinesq equation," *Results in Physics*, vol. 19, Article ID 103525, 2020.

[28] M. M. Hossain, A. Abdeljabbar, H. O. Roshid, M. M. Roshid, and A. N. Sheikh, "Abundant bounded and unbounded solitary, periodic, rogue-type wave solutions and analysis of parametric effect on the solutions to nonlinear klein-gordon model," *Complexity*, vol. 2022, Article ID 8771583, 19 pages, 2022.

[29] K. K. Ali, M. S. Osman, and M. Abdel-Aty, "New optical solitary wave solutions of Fokas-Lenells equation in optical fiber via Sine-Gordon expansion method," *Alexandria Engineering Journal*, vol. 59, no. 3, pp. 1191–1196, 2020.

[30] Y.-L. Ma, "*N*th-order rogue wave solutions for a variable coefficient Schrödinger equation in inhomogeneous optical fibers," *Optik*, vol. 251, Article ID 168103, 2022.

[31] R. Zhang, M. Shakeel, Attaullah, N. B. Turki, N. A. Shah, and S. M. Tag, "Novel analytical technique for mathematical model representing communication signals: a new travelling wave solutions," *Results in Physics*, vol. 51, Article ID 106576, 2023.

[32] M. Shakeel, Q. M. Ul-Hassan, and J. Ahmad, "Applications of the novel (G'/G)-expansion method for a time fractional simplified modified Camassa-Holm (MCH) equation," *Abstract and Applied Analysis*, vol. 2014, Article ID 601961, 16 pages, 2014.

[33] M. Shakeel, Attaullah, N. A. Shah, and J. D. Chung, "Modified exp-function method to find exact solutions of microtubules nonlinear dynamics models," *Symmetry*, vol. 15, no. 2, Article ID 360, 2023.

[34] M. Shakeel, N. A. Shah, and J. D. Chung, "Application of modified exp-function method for strain wave equation for finding analytical solutions," *Ain Shams Engineering Journal*, vol. 14, no. 3, Article ID 101883, 2023.

[35] N. Mahak and G. Akram, "Exact solitary wave solutions by extended rational sine-cosine and extended rational sinh-cosh techniques," *Physica Scripta*, vol. 94, no. 11, Article ID 115212, 2019.

[36] K. Hosseini, P. Mayeli, and R. Ansari, "Modified Kudryashov method for solving the conformable time-fractional Klein-Gordon equations with quadratic and cubic nonlinearities," *Optik*, vol. 130, pp. 737–742, 2017.

[37] S. Z. Hassan and M. A. E. Abdelrahman, "A Riccati–Bernoulli sub-ODE method for some nonlinear evolution equations," *International Journal of Nonlinear Sciences and Numerical Simulation*, vol. 20, no. 3-4, pp. 303–313, 2019.

[38] M. S. Osman, A. Korkmaz, H. Rezazadeh, M. Mirzazadeh, M. Eslami, and Q. Zhou, "The unified method for conformable time fractional Schrödinger equation with perturbation terms," *Chinese Journal of Physics*, vol. 56, no. 5, pp. 2500–2506, 2018.

[39] M. S. Osman, D. Baleanu, A. R. Adem, K. Hosseini, M. Mirzazadeh, and M. Eslami, "Double-wave solutions and Lie symmetry analysis to the (2+1)-dimensional coupled Burgers equations," *Chinese Journal of Physics*, vol. 63, pp. 122–129, 2020.

[40] M. M. Roshid, M. M. Rahman, M. H. Bashar, M. M. Hossain, and M. A. Mannaf, "Dynamical simulation of wave solutions for the M-fractional Lonngren-wave equation using two distinct methods," *Alexandria Engineering Journal*, vol. 81, pp. 460–468, 2023.

[41] M. I. Asjad, M. Manzoor, W. A. Faridi, and S. Z. Majid, "Precise invariant travelling wave soliton solutions of the Nizhnik-Novikov–Veselov equation with dynamic assessment," *Optik*, vol. 294, Article ID 171438, 2023.

[42] M. I. Asjad, S. Z. Majid, W. A. Faridi, and S. M. Eldin, "Sensitive analysis of soliton solutions of nonlinear Landau-Ginzburg-Higgs equation with generalized projective Riccati method," *AIMS Mathematics*, vol. 8, no. 5, pp. 10210–10227, 2023.

[43] N. Ullah, M. I. Asjad, A. Hussanan et al., "Novel waves structures for two nonlinear partial differential equations arising in the nonlinear optics via Sardar-subequation method," *Alexandria Engineering Journal*, vol. 71, pp. 105–113, 2023.

[44] T. Mathanaranjan, "An effective technique for the conformable space-time fractional cubic-quartic nonlinear Schrodinger equation with different laws of nonlinearity," *Computational Methods for Differential Equations*, vol. 10, no. 3, pp. 701–715, 2022.

[45] T. Mathanaranjan, "Optical solitons and stability analysis for the new (3+1)-dimensional nonlinear Schrödinger equation," *Journal of Nonlinear Optical Physics & Materials*, vol. 32, no. 2, Article ID 2350016, 2023.

[46] T. Mathanaranjan, "New jacobi elliptic solutions and other solutions in optical metamaterials having higher-order dispersion and its stability analysis," *International Journal of Applied and Computational Mathematics*, vol. 9, no. 5, Article ID 66, 2023.

[47] M. M. Roshid and H.-O. Roshid, "Exact and explicit traveling wave solutions to two nonlinear evolution equations which describe incompressible viscoelastic Kelvin-Voigt fluid," *Heliyon*, vol. 4, no. 8, Article ID e00756, 2018.

[48] M. M. Roshid, T. Bairagi, Harun-Or-Roshid, and M. M. Rahman, "Lump, interaction of lump and kink and solitonic solution of nonlinear evolution equation which describe incompressible viscoelastic Kelvin–Voigt fluid," *Partial Differential Equations in Applied Mathematics*, vol. 5, Article ID 100354, 2022.

[49] G. U. Varieschi, "Applications of fractional calculus to newtonian mechanics," *Journal of Applied Mathematics and Physics*, vol. 6, no. 6, pp. 1247–1257, 2018.

[50] D. Kumar and D. Baleanu, "Fractional calculus and its applications in physics," *Frontiers in Physics*, vol. 7, Article ID 81, 2019.

[51] E. A. Algehyne, M. S. Aldhabani, M. Areshi, E. R. El-Zahar, A. Ebaid, and H. K. Al-Jeaid, "A proposed application of fractional calculus on time dilation in special theory of relativity," *Mathematics*, vol. 11, no. 15, Article ID 3343, 2023.

[52] H. Sun, Y. Zhang, D. Baleanu, W. Chen, and Y. Chen, "A new collection of real world applications of fractional calculus in science and engineering," *Communications in Nonlinear Science and Numerical*, vol. 64, pp. 213–231, 2018.

[53] J. Ke, Y. Duan, C. Xu, and Y. Zhang, "Cross-correlation multifractal analysis of technological innovation, financial market and real economy indices," *Fractal and Fractional*, vol. 7, no. 3, Article ID 267, 2023.
[54] Y. Li, "Multifractal characteristics of China's stock market and slump's fractal prediction," *Fractal and Fractional*, vol. 6, no. 9, Article ID 499, 2022.
[55] C. Ionescu, A. Lopes, D. Copot, J. A. T. Machado, and J. H. Bates, "The role of fractional calculus in modeling biological phenomena: a review," vol. 51, pp. 141–159, Communications in Nonlinear Science and Numerical Simulation, 2017.
[56] K. C. Basak, P. C. Ray, and R. K. Bera, "Solution of non-linear Klein-Gordon equation with a quadratic non-linear term by Adomian decomposition method," *Communications in Nonlinear Science and Numerical*, vol. 14, no. 3, pp. 718–723, 2009.
[57] K. Sirendaoreji, "Auxiliary equation method and new solutions of Klein-Gordon equations," *Chaos, Solitons & Fractals*, vol. 31, no. 4, pp. 943–950, 2007.
[58] N. Hayashi and P. I. Naumkin, "Quadratic nonlinear Klein-Gordon equation in 2d, cauchy problem," *Advanced Studies in Pure Mathematics*, vol. 64, pp. 89–100, 2015.
[59] S. Zhang, "Exp-function method for Klein–Gordon equation with quadratic nonlinearity," *Journal of Physics: Conference Series*, vol. 96, Article ID 012002, 2008.
[60] X. Wang, H. Ehsan, M. Abbas, G. Akram, M. Sadaf, and T. Abdeljawad, "Analytical solitary wave solutions of a time-fractional thin-film ferroelectric material equation involving beta-derivative using modified auxiliary equation," *Results in Physics*, vol. 48, Article ID 106411, 2023.
[61] A. Atangana and R. T. Alqahtani, "Modelling the spread of river blindness disease via the caputo fractional derivative and the beta-derivative," *Entropy*, vol. 18, no. 2, Article ID 40, 2016.
[62] J. V. da C. Sousa and E. C. de Oliveira, "A new truncated M-fractional derivative type unifying some fractional derivative types with classical properties," *International Journal of Analysis and Applications*, vol. 16, no. 1, pp. 83–96, 2018.
[63] Harun-Or-Roshid, M. M. Roshid, M. M. Hossain, M. S. Hasan, M. J. H. Munshi, and A. H. Sajib, "Dynamical structure of truncated M− fractional Klein-Gordon model via two integral schemes," *Results in Physics*, vol. 46, Article ID 106272, 2023.
[64] M. M. Roshid, M. Uddin, and G. Mostafa, "Dynamical structure of optical soliton solutions for M−fractional paraxial wave equation by using unified technique," *Results in Physics*, vol. 51, Article ID 106632, 2023.
[65] T. Ak, T. Aydemir, A. Saha, and A. H. Kara, "Propagation of nonlinear shock waves for the generalised Oskolkov equation and its dynamic motions in the presence of an external periodic perturbation," *Pramana*, vol. 90, Article ID 78, 2018.
[66] M. H. Bashar and M. M. Roshid, "Rouge wave solutions of a nonlinear pseudo-parabolic physical model through the advance exponential expansion method," *International Journal of Physical*, vol. 8, no. 1, pp. 1–7, 2020.
[67] S.-W. Yao, K. U. Tariq, M. Inc, and R. N. Tufail, "Modulation instability analysis and soliton solutions of the modified BBM model arising in dispersive medium," *Results in Physics*, vol. 46, Article ID 106274, 2023.